EXPERIMENTAL AND ANALYTICAL STUDIES OF THE BEHAVIOR OF COLD-FORMED STEEL ROOF TRUSS ELEMENTS

Nuthaporn Nuttayasakul

Dissertation submitted to the Faculty of the
Virginia Polytechnic Institute and State University
in partial fulfillment for the requirements for the degree of

DOCTOR OF PHILOSOPHY
In
Civil Engineering

W. Samuel Easterling, Chairman
Thomas M. Murray
Finley A. Charney
Carin L. Roberts-Wollmann
Mehdi Setareh

November 3, 2005
Blacksburg, Virginia

Keywords: cold-formed steel, elemental test, full scale test, stub column test, flexural test, distortional buckling, local buckling

EXPERIMENTAL AND ANALYTICAL STUDIES OF THE BEHAVIOR OF COLD-FORMED STEEL ROOF TRUSS ELEMENTS

Nuthaporn Nuttayasakul

ABSTRACT

Cold-formed steel roof truss systems that use complex stiffener patterns in existing hat shape members for both top and bottom chord elements are a growing trend in the North American steel framing industry. When designing cold-formed steel sections, a structural engineer typically tries to improve the local buckling behavior of the cold-formed steel elements. The complex hat shape has proved to limit the negative influence of local buckling, however, distortional buckling can be the controlling mode of failure in the design of chord members with intermediate unbraced lengths. The chord member may be subjected to both bending and compression because of the continuity of the top and bottom chords. These members are not typically braced between panel points in a truss.

Current 2001 North American Specifications (NAS 2001) do not provide an explicit check for distortional buckling. This dissertation focuses on the behavior of complex hat shape members commonly used for both the top and bottom chord elements of a cold-formed steel truss. The results of flexural tests of complex hat shape members are described. In addition, stub column tests of nested C-sections used as web members and full scale cold-formed steel roof truss tests are reported.

Numerical analyses using finite strip and finite element procedures were developed for the complex hat shape chord member in bending to compare with

experimental results. Both elastic buckling and inelastic postbuckling finite element analyses were performed. A parametric study was also conducted to investigate the factors that affect the ultimate strength behavior of a particular complex hat shape.

The experimental results and numerical analyses confirmed that modifications to the 2001 North American Specification are necessary to better predict the flexural strength of complex hat shape members, especially those members subjected to distortional buckling. Either finite strip or finite element analysis can be used to better predict the flexural strength of complex hat shape members. Better understanding of the flexural behavior of these complex hat shapes is necessary to obtain efficient, safe design of a truss system. The results of these analyses will be presented in the dissertation.

ACKNOWLEDGEMENTS

I would like to express my gratitude to Dr. W. Samuel Easterling for his guidance and patience. I would also like to thank you Dr. Thomas M. Murray, Dr. Carin Roberts-Wollmann, Dr. Finley Charney, and Dr. Mehdi Setareh for serving on the committee.

I would also like to thank Brett Farmer and Dennis Huffman for their contribution to the fabrication and testing of the experimental part of this dissertation.

I would also like to extend my gratitude to Consolidated System Inc., which sponsored the experimental portion of this research. I would like to thank Mr. Harry Collins and Mr. Eric Jacobsen for their contribution and help with this study.

TABLE OF CONTENTS

LIST OF TABLES

LIST OF FIGURES

CHAPTER 1

INTRODUCTION

1.1 BACKGROUND

Cold-formed steel roof trusses are economical solutions for roof framing in both residential and commercial construction. The use of cold-formed steel roof truss construction has commonly been in the residential market. Due to structural, constructional and environmental advantages over timber and reinforced concrete, cold-formed steel is an attractive alternative material for many roof framing projects in both residential and commercial applications.

The use of cold-formed steel trusses has become popular during the last decade. Because of environmental awareness in the United States, building construction industries are forced to find alternatives for timber construction. Cold-formed steel has advantages over timber in terms of moisture and insect resistance. From a structural standpoint, cold-formed steel has a higher strength-to-weight ratio than timber.

Cold-formed steel trusses are commonly assembled using C-sections and self-drilling screws. Roof truss manufacturers in the United States have been trying to improve truss design by designing and producing new shapes or using complex stiffener patterns in existing shapes. Another possibility is to use nested C-sections to form a box member to improve the overall member behavior. New improvements allow the truss manufacturer to extend the application of cold-formed steel roof trusses into commercial construction applications where longer spans may be required.

1.2 STATEMENT OF PROBLEM

Cold-formed steel roof truss design relies on the strength evaluation of individual members. The basis for these calculations is described in the 2001 North American Specifications (NAS 2001). Previous researchers have reported that the predictions of strength of single C-section web members in compression and complex hat shape chord members in bending are unconservative in some cases (Schafer 2002b). These C-sections and complex hat shape are typically used as the web and chord members respectively. Therefore, design of the mentioned members using the NAS 2001 could lead to unconservative cold-formed steel truss design in some cases.

Schafer (2002b) suggested the Direct Strength Method (DSM) as a new approach to member design. The DSM uses the finite strip method as the analytical tool to calculate the elastic buckling stress, which in turn is used in the design equations to predict the inelastic buckling capacity of the member. The DSM also considers the distortional mode of buckling, which is not typically considered in the design procedures (NAS 2001).

The DSM method has proved to be an effective tool to predict the compressive and laterally braced flexural strength of typical cold-formed steel members (Schafer 2002b). Studies of the effectiveness of the DSM to predict the strength of laterally unbraced flexural members have been very limited. A complex hat shape chord member in a cold-formed steel truss, as shown in Fig. 1.1, may experience a bending moment and could be considered laterally unbraced between panel points or at the overhang where the top chord member extends beyond the end support. Therefore, further investigations on the laterally unbraced flexural strength of these members are needed.

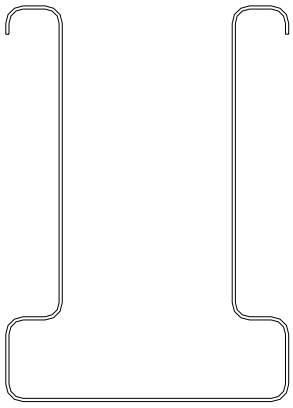

Figure 1.1 Typical Complex Hat Shape as Chord Member

The use of the nested C-sections, as shown in Fig. 1.2, to form a box member is a new trend to improve the overall strength and efficiency of the web member in truss design. There has been no report on either experimental or analytical studies on the compressive strength of the nested C-sections. Stub column tests are required by the NAS 2001 for strength determination. Numerical analyses can be used to determine the strength at longer lengths. Analytical tools, such as the finite element method, can be used to improve the design of the nested C-sections.

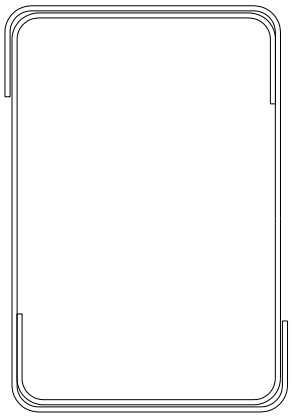

Figure 1.2 Built-Up Nested Channel Section

1.3 OBJECTIVE & SCOPE

The four main objectives of the research are as follows:

1. Experimentally evaluate the Consolidated Systems, Inc. cold-formed steel roof truss system including the truss-to-truss connections, end anchorage devices, chord and web members as well as the complete truss assembly.

2. Experimentally and analytically evaluate the behavior of built-up compression members made of nested C-sections to form a box member.

3. Improve the flexural design for laterally un-braced cold-formed steel beams using complex hat shapes.

4. Evaluate the overall truss behavior and design methodology through complete truss tests and analysis.

The scope of the research is as follows:

1. Stub-column tests were performed and results were compared with analytical calculations according to the NAS 2001.

2. Laterally unbraced flexural tests for the complex hat shape chord members were performed and results were compared with analytical calculations according to the NAS 2001 and the DSM. Finite strip analyses were used to determine the appropriate lengths for the test specimens. Local, distortional, and flexural torsional buckling behavior were investigated. Parametric studies using finite element analyses were used to investigate the effects of the geometric imperfection and material nonlinearity.

3. Tests of a complete cold-formed steel roof truss were performed. Instrumentation on web members and chord members was used to monitor the member forces. The trusses are intended for commercial buildings and the test specimens had a span of 52 feet. Results from both the elemental tests and the full-scale tests were analyzed to evaluate the design methodology for the cold-formed steel truss.

1.4 ORGANIZATION OF THIS DISSERTATION

The Literature review of related research is reported in Chapter 2. Stub column tests and analyses for web members are reported in Chapter 3. Laterally unbraced flexural tests and finite strip analyses for chord members are reported in Chapter 4. The comparisons between the finite strip analyses and tests were used to investigate the effectiveness of the finite strip method. The complete truss tests were performed on 52 ft span cold-formed steel roof trusses and reported in Chapter 5. The comparison between the complete truss experimental results and the predicted values are reported. The Finite element analyses of the chord members in bending are reported in Chapter 6. The finite element analyses were performed for both elastic and inelastic models. The effects of material and geometric nonlinearity were investigated and reported. Chapter 7 summarizes the dissertation and provides conclusions and suggestions for future research.

CHAPTER 2

LITERATURE REVIEW

2.1 INTRODUCTION

Hancock et al. (2001) described three basic buckling modes for cold-formed steel member as local, distortional, and overall buckling as shown in Fig. 2.1. The local buckling mode involves only plate flexure within the line junctions between adjacent plates, which remain straight. Distortional buckling is a buckling mode in which the lip-stiffened elements of the section rotate about the flange-web junction. The overall mode involves translation of cross sections of the member without section distortion. The overall mode may consist of simple column (Euler) buckling or flexural-torsional buckling.

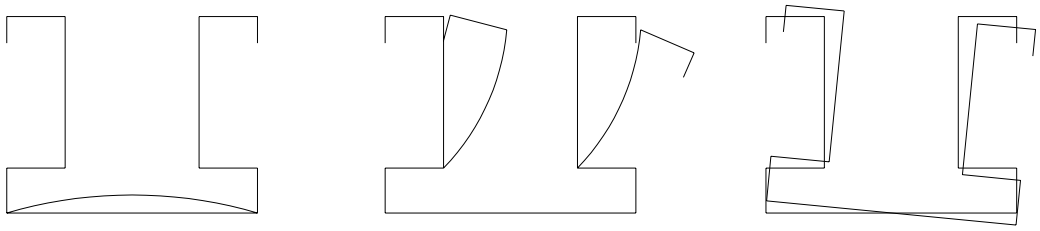

Local Distortional Flexural-torsional

Figure 2.1 Three Basic Buckling Modes

2.2 COLD-FORMED STEEL COLUMNS

Kwon and Hancock (1992) reported that thin-walled channel sections and other sections of a singly-symmetric profile, such as hat sections, may undergo distortional buckling. Kwon and Hancock performed experimental tests and

analytical studies on channel columns undergoing local and distortional buckling. The analyses were done using the BFINST program developed by Hancock to perform a finite strip analysis. The authors argued that Winter's (1968) formula could also be used to predict the compressive strength of tested channel undergoing distortional buckling. The Winter (1968) formula can be expressed as follows.

$$\frac{b_e}{b} = \sqrt{\frac{\sigma_l}{F_y}}\left(1 - 0.22\sqrt{\frac{\sigma_l}{F_y}}\right) \tag{2.1}$$

where b_e = the effective part of the plate width b

F_y = yield stress of the steel

σ_l = the elastic local buckling stress

Winter's equation is based on local buckling of single plate. If the elastic local buckling stress (σ_l) is replaced by the elastic distortional buckling stress (σ_{de}), then the modified Winter's equation for distortional buckling can be expressed as follows.

$$\frac{b_e}{b} = 1 \qquad \lambda \leq 0.673 \tag{2.2}$$

$$\frac{b_e}{b} = \sqrt{\frac{\sigma_{de}}{F_y}}\left(1 - 0.22\sqrt{\frac{\sigma_{de}}{F_y}}\right) \qquad \lambda > 0.673 \tag{2.3}$$

where σ_{de} = elastic distortional buckling stress

$$\lambda = \sqrt{\frac{F_y}{\sigma_{de}}}$$

Winter's equation was found to be unconservative when compared with the column test results of cold-formed channels conducted by Kwan and Hancock (1992), therefore, they proposed the following equations that agrees better with their test results.

$$\frac{b_e}{b} = 1 \qquad \lambda \leq 0.561 \qquad (2.4)$$

$$\frac{b_e}{b} = \left(\frac{\sigma_{de}}{F_y}\right)^{0.6}\left(1 - 0.25\left(\frac{\sigma_{de}}{F_y}\right)^{0.6}\right) \qquad \lambda > 0.561 \qquad (2.5)$$

Note that Eqs. 2.4 and 2.5 are referred to hereafter the Hancock equations.

Winter's and Hancock's equations are plotted as shown in Figure 2.2. Although the test data is not shown on this plot, Kwon and Hancock (1992) showed that Eq. 2.5 agrees with test results better than Eq. 2.1.

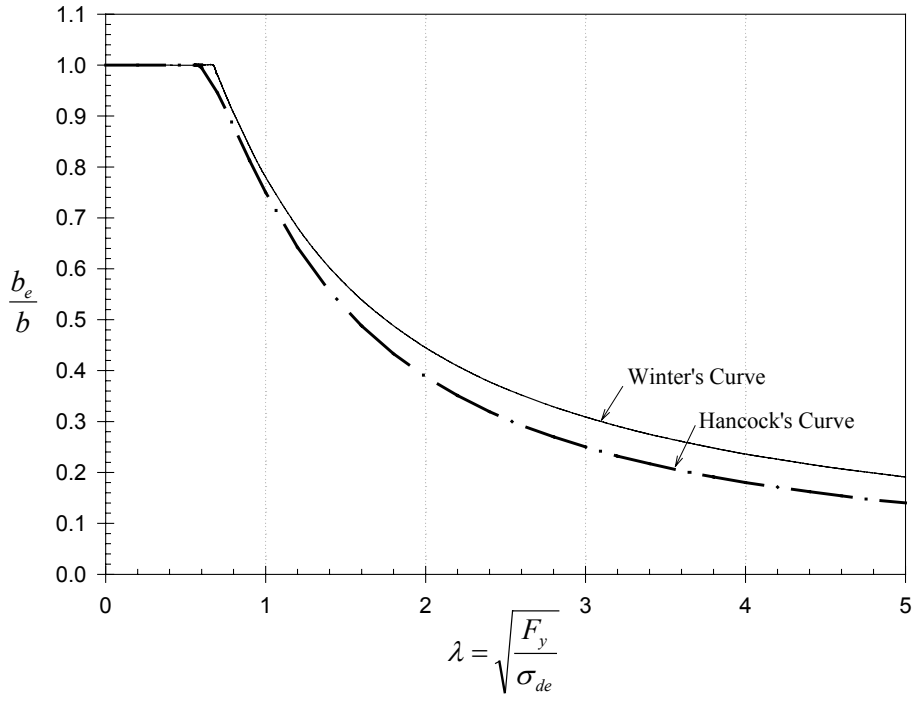

Figure 2.2 Winter and Hancock Curves

Polyzois and Charnvarnichborikarn (1993) performed experiments on Z-sections under compression. The findings showed that the distortional failure of the flange/lip component may be the limit state of the section. The distortional mode has very little postbuckling strength. Hancock et.al. (1994) reported that some deck and rack sections may also undergo distortional buckling. The additional finding from his previous work in 1992 was that there is no adverse interaction between local and distortional buckling. Therefore, the distortional buckling strength can be assessed independently of the local buckling strength even when local buckling is occurring simultaneously.

Schafer (2002b) reported that the 1996 AISI design Specifications for cold-formed steel columns ignore local buckling interaction with the flexural or flexural torsional buckling and do not provide an explicit check for distortional mode. Numerical analyses and experimental results indicate that postbuckling capacity in the distortional mode is lower than in the local mode. This finding implies that the member may fail in the distortional mode even when the stress required at failure for the elastic distortional buckling mode is higher than the elastic local buckling mode.

2.3 COLD-FORMED STEEL FLEXURAL MEMBERS

Schafer and Pekoz (1999) investigated laterally braced cold-formed steel flexural members with edge stiffened flanges. The edge stiffened flange is described as a flange that is stiffened by a lip at the end of flange. Their findings showed that the moment capacity is affected by local or distortional buckling. The distortional mode was considered to have heightened imperfection sensitivity and lower postbuckling capacity than the local buckling mode. Their findings include the gathering of experimental work from many researchers and analyzing the data considering distortional buckling. They proposed design provisions that integrate distortional buckling into the unified effective width approach currently used in

NAS (2001). All the test data gathered were from laterally braced flexural members.

Experimental studies focusing on laterally unbraced cold-formed steel flexural members have been very limited. A key piece of existing literature is a study by Baur and LaBoube (2001) that documents the results of an experimental evaluation of complex hat shapes from different truss manufacturers. In this study, the authors conclude that, depending on the unbraced lengths, these shapes experience distortional buckling. The 1996 AISI Specifications do not explicitly address the general limit state of distorsional buckling, but do refer to it in the commentary of section C3.1.2. The experimental studies by Baur and LaBoube (2001) showed that ignoring the limit state of distortional buckling can be unconservative.

Baur and LaBoube used the finite strip method described by Schafer (2002b) to determine the critical buckling stress. This buckling stress is in turn used with Eqs. 2.2-2.5 to predict the inelastic buckling stress. The Winter and Hancock curves provide good correlation with the experimental results for beams with an unbraced length of 2 to 4 ft.

The methods utilized by Baur and LaBoube can also be described in Eqs. 2.6-2.9 using moment terms instead of stress. The yield moment (M_y) is based on the full section modulus. The elastic distortional buckling moment (M_{crd}) is based on the finite strip analysis. The expression represented by Eqs. 2.6 and 2.7 were presented by Kwon and Hancock (1992) and are attributed to Winter (1968). The inelastic distortional moment capacity (M_{nd}) is given by

For $\lambda_d \leq 0.673$ $\qquad M_{nd} = M_y$ (2.6)

For $\lambda_d > 0.673$ $\qquad M_{nd} = \left(1 - 0.22\left(\frac{M_{crd}}{M_y}\right)^{0.5}\right)\left(\frac{M_{crd}}{M_y}\right)^{0.5} M_y$ (2.7)

where $\lambda_d = \sqrt{M_y / M_{crd}}$

M_{crd} = Critical elastic distortional buckling moment

Kwon and Hancock (1992) proposed modified equations to better fit the experimental data. These are expressed by:

For $\lambda_d \leq 0.561$ $\quad M_{nd} = M_y$ (2.8)

For $\lambda_d > 0.561$ $\quad M_{nd} = \left(1 - 0.25\left(\frac{M_{crd}}{M_y}\right)^{0.6}\right)\left(\frac{M_{crd}}{M_y}\right)^{0.6} M_y$ (2.9)

Baur and LaBoube (2001) reported that the Kwon and Hancock equations have a better correlation and are more conservative when compared with the experimental results.

2.4 FINITE STRIP METHOD

The finite strip method was first developed by Cheung (1976). The finite strip technique used in the cold-formed steel application is referred to as the spline finite strip method. The spline finite strip method was initially developed for the analysis of plate and shell structures. Cheung and Tham (1997) thoroughly present the theory behind the finite strip method. Hancock modified the stiffness matrices derived by Cheung (1976) and extended the technique for cold-formed steel members. The use of the finite strip method as a design tool is described in detail by Hancock, et al (2001).

The software utilizing the spline finite strip is readily available on different platforms. Hancock (1978) developed BFINST for use in the finite strip method calculations. The DOS based platform of the BFINST program makes it hard to extend and further develop in research. Schafer (2002b) introduced the freeware

version based on the Matlab platform called CUFSM. This program is easier to use and further develop in a research environment.

2.5 DIRECT STRENGTH METHOD

Schafer (2002b) collected and reported data from several studies on columns and laterally braced beams. The data from these studies were used to calibrate the Direct Strength Method (DSM) proposed by Schafer as a new approach for the cold-formed steel design standard. The direct strength method employs elastic buckling calculations using rational analysis. These elastic buckling calculations are used to calibrate the equations used to predict the inelastic behavior of the cold-formed steel members.

The axial strength of cold-formed steel columns, when the column is concentrically loaded with pin-ended conditions, as well as the flexural strength of cold-formed steel beams can be predicted using the DSM. The design philosophy is based on the fact that cold-formed steel member may have three competing mode of failures. The first mode of failure is the flexural, torsional or flexural-torsional buckling. The second mode is local buckling and the third mode is distortional buckling.

2.5.1 COLUMN STRENGTH

The calculations used to determine the axial compressive strength using the DSM are given in the following sections.

2.5.1.1 FLEXURAL, TORSIONAL, OR FLEXURAL-TORSIONAL BUCKLING

The nominal axial strength, P_{ne}, for flexural, torsional, or flexural-torsional buckling is

For $\lambda_c \leq 1.5$ $\quad P_{ne} = \left(0.658^{\lambda_c^2}\right) P_y$ (2.10)

For $\lambda_c > 1.5$ $\quad P_{ne} = \left(\frac{0.877}{\lambda^2_c}\right) P_y$ (2.11)

where $\lambda_c = \sqrt{P_y / P_{cre}}$

$P_y = A_g F_y$

P_{cre} = Minimum of the critical elastic column buckling load in flexural, torsional, or flexural-torsional buckling (NAS 2001)

2.5.1.2 LOCAL BUCKLING

The nominal axial strength, P_{nl}, for local buckling is

for $\lambda_d \leq 0.776$ $\quad P_{nl} = P_{ne}$ (2.12)

for $\lambda_d > 0.776$ $\quad P_{nl} = \left(1 - 0.15\left(\frac{P_{crl}}{P_{ne}}\right)^{0.4}\right)\left(\frac{P_{crl}}{P_{ne}}\right)^{0.4} P_{ne}$ (2.13)

where $\lambda_l = \sqrt{P_{ne} / P_{crl}}$

P_{crl} = Critical elastic local column buckling load
(using finite strip analysis)

2.5.1.3 DISTORTIONAL BUCKLING

The nominal axial strength, P_{nd}, for distortional buckling is

for $\lambda_d \leq 0.561$ $\quad P_{nd} = P_y$ (2.14)

for $\lambda_d > 0.561$ $\quad P_{nd} = \left(1 - 0.25\left(\frac{P_{crd}}{P_y}\right)^{0.6}\right)\left(\frac{P_{crd}}{P_y}\right)^{0.6} P_y$ (2.15)

where $\lambda_d = \sqrt{P_{ne}/P_{crd}}$

P_{crd} = Critical elastic distortional column buckling load
(using finite strip analysis)

The strength of the column is the minimum of the calculations from the P_{ne}, P_{nl}, and P_{nd}. The DSM method provides acceptable reliability for predicting the axial strengths of concentrically loaded, pin-ended cold-formed steel columns (Schafer 2002b).

2.5.2 FLEXURAL STRENGTH

Schafer (2002b) has also conducted extensive studies on the flexural behavior of cold-formed steel sections. Most of the efforts to verify the local and distortional buckling predictions were concentrated on laterally braced flexural members, because these were traditionally deemed to be the most applicable bracing configuration. The tests on laterally braced members such as Z-section purlins were used to calibrate the DSM predictions of the local and distortional buckling sections. The overall mode can be predicted by currently used predictions in the NAS (2001). The flexural strength equations using the DSM for cold-formed steel beams are summarized in the following sections.

2.5.2.1 LATERAL-TORSIONAL BUCKLING

The nominal flexural strength, M_{ne}, for lateral-torsional buckling is

for $M_{cre} < 0.56M_y$ $\quad M_{ne} = M_{cre}$ (2.16)

for $2.78M_y \geq M_{cre} \geq 0.56M_y$ $\quad M_{ne} = \frac{10}{9} M_y \left(1 - \frac{10M_y}{36M_{cre}}\right)$ (2.17)

for $M_{cre} > 2.78M_y$ $\quad M_{ne} = M_y$ (2.18)

where

$M_y = S_g F_y$, where S_g is referenced to the extreme fiber in first yield

M_{cre} = Critical elastic lateral-torsional buckling moment (NAS 2001)

2.5.2.2 LOCAL BUCKLING

The nominal flexural strength, M_{nl}, for local buckling is

For $\lambda_l \leq 0.776$ $\quad M_{nl} = M_{ne}$ (2.19)

For $\lambda_l > 0.776$ $\quad M_{nl} = \left(1 - 0.15\left(\frac{M_{crl}}{M_{ne}}\right)^{0.4}\right)\left(\frac{M_{crl}}{M_{ne}}\right)^{0.4} M_{ne}$ (2.20)

Where $\lambda_l = \sqrt{M_{ne}/M_{crl}}$

M_{crl} = Critical elastic local buckling moment
(using finite strip analysis)

2.5.2.3 DISTORTIONAL BUCKLING

The nominal flexural strength, M_{nd}, for distortional buckling is

For $\lambda_d \leq 0.673$ $\quad M_{nd} = M_y$ (2.21)

For $\lambda_d > 0.673$ $\quad M_{nd} = \left(1 - 0.22\left(\frac{M_{crd}}{M_y}\right)^{0.5}\right)\left(\frac{M_{crd}}{M_y}\right)^{0.5} M_y$ (2.22)

Where $\lambda_d = \sqrt{M_y/M_{crd}}$

M_{crd} = Critical elastic distortional buckling moment
(using finite strip analysis)

The strength of the beam is the minimum of the calculations from the M_{ne}, M_{nl}, and M_{nd}. The DSM method on predicting local and distortional buckling provides acceptable reliability for predicting the flexural strengths of laterally braced flexural members (Schafer 2002b). Additional data is needed to evaluate laterally unbraced flexural members using the DSM before local and distortional buckling predictions using the DSM can be applied effectively.

2.6 TRUSS DESIGN

LaBoube and Yu (1998) reported on recent research and development of cold-formed steel framing at the University of Missouri-Rolla (UMR). The report indicated that steel trusses in the residential construction market are commonly assembled using C-shaped sections and self-drilling screw. Ibrahim (1998) conducted experimental studies at UMR on cold-formed C-section residential trusses. Based on UMR research findings, recommendations from research were adopted into the standard for cold-formed steel framing- truss design (AISI/COFS/TRUSS 2001). The important findings are as follows:

a. Top and bottom chord members should be modeled as continuous at intermediate panel points and pin-ended at end panel points
b. Web member connections should be modeled as pin connections
c. C-section compression webs behave as beam-columns and exhibit only a flexural buckling failure mode.
d. The use of 0.85 end moment coefficient (C_m) and an effective length factor of 0.75 for the design of continuous top chords yield a good comparison with the experimental results

The end moment coefficient and an effective length factor used in the standard for cold-formed steel framing- truss design (AISI/COFS/TRUSS 2001) are based on

C-section trusses. However, the same values are recommended for hat-shape chord members.

2.7 COMPUTATIONAL MODELING

Pekoz and Schafer (1998) have shown that modeling assumptions in the computational models of cold-formed steel members are important. Pekoz and Schafer (1998) reported preliminary guidelines for computational modeling of cold-formed members, including the modeling of imperfections and residual stresses. These fundamental quantities for characterizing the geometric imperfections and residual stresses are necessary for accurate analyses and parametric studies of cold-formed steel members.

The geometric imperfections are the deviations of a member from its original idealized geometry. Pekoz and Schafer (1998) collected data on geometric imperfections from previous research. These data can be categorized into the maximum local imperfection in a stiffened element (type1) and the maximum deviation from straightness for a lip stiffened or unstiffened flange (type2) as shown in Fig. 2.3. The strength of cold-formed steel members is particularly sensitive to imperfections in the shape of its eigenmodes, especially the lowest eigenmode. Therefore, the maximum amplitude of imperfections used in the lowest eigenmodes is a conservative approach to describe the governing imperfections. As a rule of thumb, the type 1 imperfections can be approximated as

$$d_1 \approx 0.006w \quad \text{where } w = \text{width} \tag{2.23}$$

For type 2 imperfections, the maximum deviation can be approximated as

$$d_2 \approx t \qquad \text{where } t = \text{thickness} \qquad (2.24)$$

In modeling the residual stresses, the average value in percentage of the yield stress can be used to include the effect in the analyses. The average values recommended by Pekoz and Schafer (1998) are shown in Fig. 2.4 for both roll-formed and press-braked cold-formed steel. These quantities include both membrane and flexural residual stress effects.

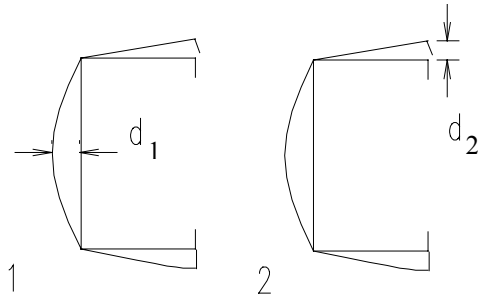

Figure 2.3 Geometric Imperfection (Pekoz and Schafer, 1998)

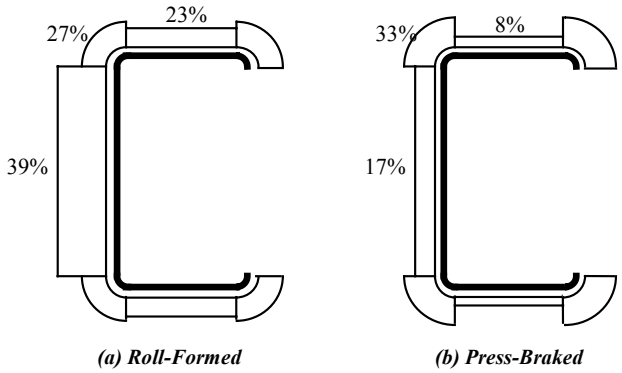

Figure 2.4 Residual Stresses in $\%f_y$ (Pekoz and Schafer, 1998)

Shanmugam and Dhanalakshmi (2000) investigated perforated cold-formed steel angles used as compression members. A comparison of the test results and the

finite element model showed that the finite element model is capable of predicting the strength and the failure modes with reasonable accuracy. The analyses were performed using the ABAQUS finite element package. The authors used element type S8R5, which is an 8-noded, double curved thin shell with reduced integration and five degrees of freedom per node. The results showed that the prediction of the ultimate load by FEA is within 10%, but generally higher, than the experimental results. The authors explained that the difference may be due to the approximation of the material and geometric nonlinearity used in the plate elements without openings.

Young and Yan (2002) investigated cold-formed steel channel columns undergoing local, distortional, and overall buckling. The authors concluded that the finite element model closely predicted the experimental ultimate loads and the behavior of the cold-formed channel columns. The FEA model includes the effect of geometric imperfections by using a linear perturbation analysis. Linear analysis can be used to establish the probable buckling modes of the column. The buckling mode or eigenmode was scaled by a factor to obtain a perturbed mesh of the column for the nonlinear analysis. The displacement control loading method was used with the S4R5 element in ABAQUS, which as previously noted, is an 8-noded, double curved thin shell with reduced integration and five degrees of freedom per node. The parametric study also showed that the AISI Specification is unconservative in some cases. This is not the case for the Australian Standard (AS/NZS 1996) because it includes a separate check for distortional buckling of singly symmetric sections.

2.8 APPLICATION OF PRIOR RESEARCH TO THE CURRENT PROJECT

Previous analytical research on cold-formed steel roof trusses has been very limited. The published research concentrated on C-shaped sections used in residential construction market (LaBoube and Yu 1998). The introduction of

complex hat shapes for chord members and nested C-shaped sections for web members has raised a question as to whether the previous findings can be applied to this new development. The stub column tests for nested C-shaped section web members and flexural tests for complex hat shape chord members are necessary to provide test data for comparison with predictions discussed in the literature review. The complete truss test, with complex hat shape chord members and nested C-shaped web members, can add additional information on truss design and development to the currently limited database. Finally, recommendations from previous research on finite element analyses of cold-formed steel members can be used to create finite element models of complex hat shape chord members in bending. The finite element analyses can be used to further evaluate the test results and investigate the flexural behavior of complex hat shape chord members.

CHAPTER 3

STUB COLUMN TESTS OF WEB MEMBERS

3.1 INTRODUCTION

This chapter presents the results of 23 fixed-ended stub column tests performed on built-up cold-formed members consisting of nested C-sections and single C-sections. The objective of this portion of the study is to confirm the stub column test data and the comparison between the test results and predicted values using the NAS (2001). For built-up members consisting of nested C-sections, the available data is very limited. According to Schafer (2002a), the single channel used as a compression member is subjected to at least three competing buckling modes: local, distortional, and flexural buckling. The web members of a built-up roof truss consisting of nested channels can improve the behavior of the section under compression load because of improved rigidity. When proper restraint, such as adequate screw spacing, is provided to prevent the separation of each member, the failure mode can be limited to the inelastic local buckling.

3.2 TEST SPECIMENS

Both built-up sections, consisting of nested channels as shown in Fig. 3.1, and single C-sections were tested. Two channels are nested together to form a hollow box section. The individual channels were simple lipped sections with a lip stiffener size, d, of 0.375 in. and typical inside bend radius, R, of 0.12 in. The section depths, D, ranged from 2.5 in. to 6.0 in. and the width, B, ranged from 1.5 in. to 2.0 in. The test specimen cross sections are summarized in Table 3.1. The BW sections and C sections stands for built-up web and single C-shaped web respectively. The specimen lengths were chosen using the recommendation of

Galambos (1998), that is, the length should be more than three times the largest dimension but less than twenty times the radius of gyration, $r_{y,}$ of the tested section. Based on those criteria, the specimen lengths were determined as shown in Table 3.2. The specimens were milled at both ends to achieve the required flatness. A wooden block was inserted into the built-up member to prevent damage of the specimen's ends during the milling process.

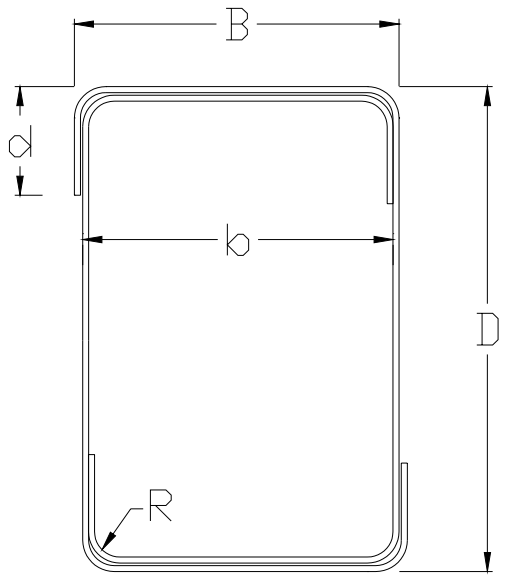

Figure 3.1 Built-Up Nested Channel Section

Table 3.1 The Geometric Properties of the Tested Sections

Designation	Gage	Inside Bend Radius, R (in.)	Lip d (in.)	Thickness t (in.)	Depth D (in.)	Width B (in.)	Inside Width b (in.)
BW250x150	18	0.120	0.375	0.045	2.5	1.5	1.40
BW250x200	18			0.045	2.5	2.0	1.90
BW400x150	18			0.045	4.0	1.5	1.40
BW400x200	18			0.045	4.0	2.0	1.90
BW600x150	20			0.035	6.0	1.5	1.40
BW600x200	20			0.035	6.0	2.0	1.90
C250x150	20			0.035	2.5	1.5	N/A
C250x200	22			0.028	2.5	2.0	N/A

Note: BW = Built-up web member
C = Single C-shaped web member

Table 3.2 The Summary of the Tested Specimens Length

Designation	Largest Dimension, D (in.)	Smallest Radius of Gyration, r_y(in.)	D*L	20*r_y	Length Tested (in.)
BW250x150	2.5	0.576	7.5	11.52	10
BW250x200	2.5	0.751	7.5	15.02	10
BW400x150	4	0.604	12	12.08	12
BW400x200	4	0.792	12	15.85	12
BW600x150	6	0.636	18	12.71	18
BW600x200	6	0.835	18	16.70	18
C250x150	2.5	0.556	7.5	11.12	8
C250x200	2.5	0.734	7.5	14.68	8

3.3 MATERIAL PROPERTIES

The sections were formed from a steel conforming to ASTM A653 Grade 50 with a specified minimum yield strength, F_y, of 50 ksi and ultimate strength, F_u, of 65 ksi. Tensile coupon test specimens were taken from the flat width of the tested specimens. Table 3.3 summarizes the average yield strength, F_{ya}, and average ultimate strength, F_{ua}, of the specimens from three coupon tests of each thickness.

Table 3.3 The Coupon Test Results from the Tested Specimens

Gage	Average Measured Thickness (in.)	Average Yield Strength (ksi)	Average Ultimate Strength (ksi)
18	0.045	58.2	76.3
20	0.035	62.7	82.4

3.4 TEST SET-UP

The tests were conducted using a 30 kip capacity Instron Universal Testing machine. The built-up member was compressed between fixed-end flat steel plates as shown in Fig. 3.2. Four strain gages, one on each side of a built-up web member, were used to monitor and ensure the uniformity of loading on all sides of

the specimen. The loading rate was 0.004 in./min. Load increments of 10% of the expected failure load were used.

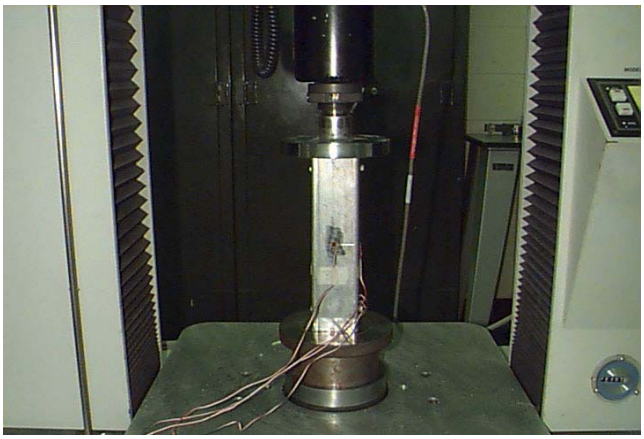

Figure 3.2 Test Set-Up

3.5 RESULTS

The ultimate loads, P_u, are summarized in Table 3.4. The ultimate loads were taken when the specimen failed to carry additional compressive load.

Table 3.4 The Summary of the Test Results

Section	Ultimate Load (kips)				% of Ultimate Load when Sign of Local Buckling Starts
	Test 1	Test 2	Test 3	Average	
BW250x150	25.64	25.26	25.81	25.57	95%
BW250x200	27.52	28.08	28.31	27.97	95%
BW400x150	25.54	23.83	24.12	24.50	65%
BW400x200	27.19	27.68	27.01	27.29	55%
BW600x150	15.33	14.98	N/A	15.16	55%
BW600x200	18.77	17.17	17.39	17.78	45%
C250x150	8.05	8.15	7.76	7.99	N/A
C250x200	5.41	5.45	5.46	5.44	N/A

The specimens designated as BW250 had a lower flat width to thickness ratio than specimens designated as BW400 and BW600. The specimen designated as BW250 did not show signs of local buckling until the load was approximately

95% of the ultimate load. The specimens designated as BW400 and BW600 demonstrated local buckling on the panel, which has the largest dimension, at approximately 45% to 65% of its ultimate strength as shown in Table 3.4. These specimens demonstrated high post buckling strengths after their first elastic buckling occurred. At the ultimate loads, all specimens failed in the inelastic local buckling mode as shown in Fig. 3.3. The nested channel section did not come apart during the test. The distortion of the material compressed the individual channel together and kept them from separation. The failures of all specimens are shown in Fig. 3.4.

Figure 3.3 Typical Inelastic Local Buckling Mode of Failure

Figure 3.4 Failure of all specimens

3.6 COMPARISON OF TEST STRENGTHS WITH DESIGN STRENGTHS

Based on the results obtained from the experimental study, the tested load, P_u, was used to calculate the effective area, $A_{e(test)}$, and compared to the nominal effective area, $A_{e(nom)}$, which is defined by the NAS (2001) section C4. The $A_{e(test)}$ values were calculated using the average ultimate loads, P_u, shown in Table 3.4 and the average yield strength, F_{ya} from the tensile coupon tests shown in Table 3.3. The $A_{e(nom)}$ values were calculated using the CFS Cold-Formed Steel Design Software version 4.14 (CFS 2004). The yield stress used in the calculation of the $A_{e(nom)}$ was taken to be the average yield strength, F_{ya} from the tensile coupon tests. The ratios between the effective areas calculated from the experimental results and the effective area calculated using the NAS (2001) are summarized in Table 3.5.

Table 3.5 Test to Predicted Ratio

Section Name	Total Area (in^2)	$A_{e(test)} = P_u / F_{ya}$ (in^2)	$A_{e(nom)}$ (in^2)	$\frac{A_{e(test)}}{A_{e(nom)}}$
BW250x150	0.516	0.439	0.394	1.12
BW250x200	0.607	0.481	0.416	1.16
BW400x150	0.652	0.421	0.408	1.03
BW400x200	0.742	0.469	0.429	1.09
BW600x150	0.643	0.252	0.273	0.92
BW600x200	0.713	0.291	0.280	1.04
C250x150	0.203	0.127	0.133	0.96
C250x200	0.195	0.087	0.100	0.86

As expected, the BW600 sections, with the highest width to thickness ratios, have the effective area approximately 40% of the total area. The BW400 sections and BW250 sections have lower width-to-thickness ratios and have the effective area approximately 65% and 80% of the total area respectively. The test results are conservative compared to the NAS (2001) except for the single C-section and the BW600x150. The single C-sections, especially the 0.045 in. specimens, show unconservative comparison. Previous research confirmed that the local and distortional buckling may have an influence on single C-sections in compression.

A method to determine the strength of single C-section in compression is proposed by Schafer (2002b).

3.7 CONCLUSIONS

Based on the stub column test results alone, the built-up channel sections satisfy the predicted design values using the NAS (2001). By using the nested channel sections, the inelastic local buckling failure mode can be achieved because of the improved torsional rigidity. The inelastic local buckling mode of failure is harder to achieve using a single channel section, which is subject to other modes of failure. Further experimental and analytical studies are needed for nested C-sections of longer lengths. The nested channel sections may separate and act as a single channel if there is not adequate restraint of members using self-drilling screws. The single C-section column strength can be better predicted using the DSM proposed by Schafer (2002b).

CHAPTER 4

LATERALLY UNBRACED FLEXURAL TESTS OF CHORD MEMBERS

4.1 INTRODUCTION

When designing cold-formed steel sections, an engineer typically tries to improve the local buckling behavior of the cold-formed steel elements. The complex hat shape has proved to limit the negative influence of local buckling, however, distortional buckling can be the controlling mode of failure in the design for flexural members with intermediate unbraced lengths. When designing a cold-formed steel truss, the chord member may induce bending moment because of the continuity of the top and bottom chord members. These members are not typically braced between each panel point in a truss. A better understanding of the flexural behavior of these complex hat shapes is necessary for improved design of a truss system.

4.2 BACKGROUND

Researchers have conducted extensive studies on the flexural behavior of cold-formed steel sections. Most of the efforts have been concentrated on laterally braced flexural members. Because cold-formed steel flexural member have traditionally been utilized in roof or floor systems, the sections have been tested primarily as fully braced flexural members. Schafer (2002b) collected data from an extensive number of tests performed on laterally braced beams. This data was used to calibrate the Direct Strength Method (DSM). The DSM method proves to provide acceptable reliability for predicting the flexural strength of laterally

braced flexural members. Laterally unbraced members, such as chords in a roof truss, are not currently address by the DSM.

4.3 EXPERIMENTAL STUDY

The objective of this part of the study is to verify and compare the flexural behavior of the cold-formed steel chord members with the NAS (2001) and the DSM. The complex hat shape, as shown in Fig. 4.1, was tested with two different thicknesses and four different geometries. Table 4.1 summarizes the measured geometric properties of the tested specimens. Based on the preliminary finite strip analyses, three different unbraced lengths were chosen at 30, 60, and 100 inches. The test set-up was a four-point bending test as shown in Fig. 4.2. The lateral braces were provided at each load point (P) by flat plates. The hydraulic rams were placed at both ends under the pinned end supports. Load cells were placed at both ends of the unbraced length (b). The end length (a) of 20 in. was chosen and used throughout all tests. The unbraced length (b) was set up at 30, 60, and 100 in. Hollow structural sections (HSS) were used to simulate the web member of the truss at the end of unbraced length (b). The HSS sections were screwed to the center of the chord member using number 10 self-drilling screws. Each specimen was loaded to failure defined as the loss of load carrying capacity.

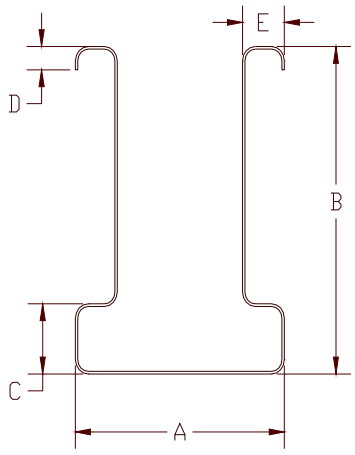

Figure 4.1 Typical Chord Member Geometry

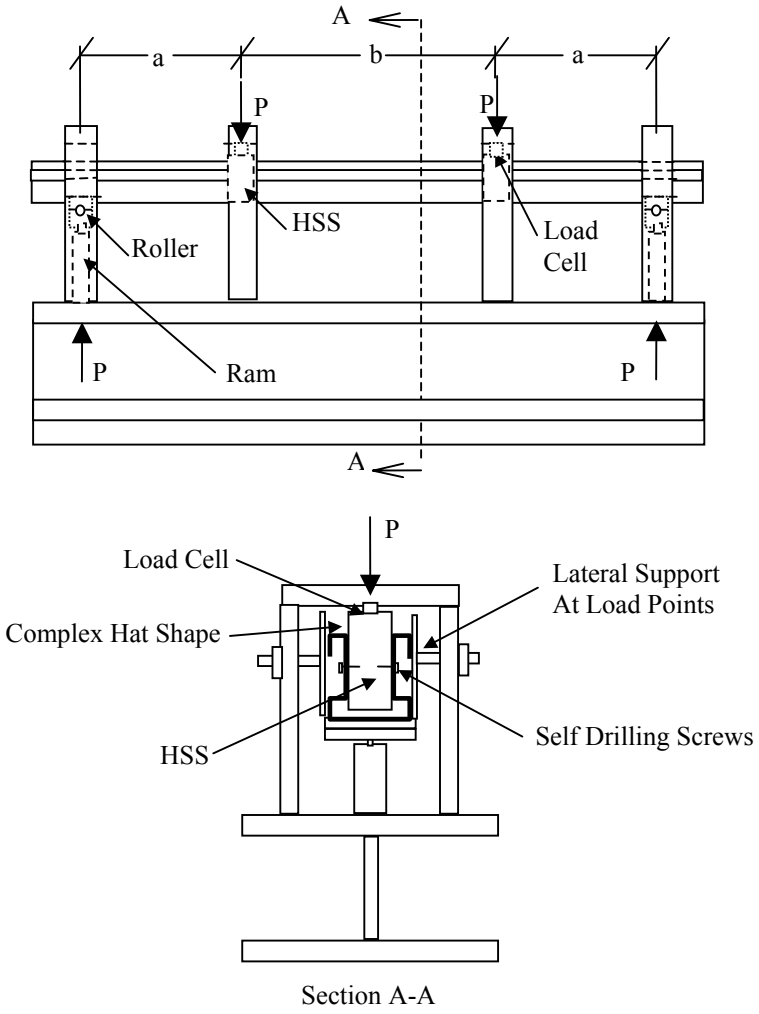

Figure 4.2 Schematic Drawing of Test Set-Up

Table 4.1 Measured Geometric Properties of Tested Sections

Designation	Thickness (in.)	Nominal Dimension (in.)					Section Modulus (in^3)
		A	B	C	D	E	
3.0x5.0-GA14	0.071	3.00	5.00	0.75	0.25	0.50	1.051
3.0x5.0-GA22	0.028	3.00	5.00	0.75	0.25	0.50	0.446
2.5x5.0-GA14	0.071	2.50	5.00	0.75	0.25	0.50	0.831
2.5x5.0-GA22	0.028	2.50	5.00	0.75	0.25	0.50	0.434
3.0x3.5-GA14	0.071	3.00	3.50	0.75	0.25	0.50	0.587
3.0x3.5-GA22	0.028	3.00	3.50	0.75	0.25	0.50	0.253
2.5x3.5-GA14	0.071	2.50	3.50	0.75	0.25	0.50	0.570
2.5x3.5-GA22	0.028	2.50	3.50	0.75	0.25	0.50	0.246

Note: All Inside Bend Radii are 0.125 in.

4.4 RESULTS

The experimental results are summarized in Table 4.2 and Table 4.3. Based on the ASTM A370 criteria, Table 4.2 shows the average values of the yield stress, ultimate stress, and percent elongation from the tensile coupon tests. Because all the sections were rolled from the same steel sheet, average values of the tensile coupon tests will be used. Table 4.3 shows the tested ultimate loads (P). Because all the distances between the hydraulic ram and the end of the unbraced length (a) are constant at 20 in., the calculation of the moment is the multiplication of P and a.

The typical failure mode of the 30-in. and 60-in. unbraced length tests was in the first distortional buckling mode shape as shown in Fig. 4.3. Two specimens, as indicated in Table 4.3, failed in the second distortional buckling mode shape. These second mode failures could be caused by the initial imperfection of the tested specimen. The plots of the first and second mode shapes of failure are from the results of finite strip analyses and shown in Fig. 4.3. The failure mode of the 60-in. unbraced length was mixed between the distortional and lateral-torsional modes. The 100-in. unbraced length tests failed in the lateral-torsional mode.

Table 4.2 Tensile Properties

	Actual Thickness (in.)	Average Yield Strength (psi)	Average Ultimate Strength (psi)	% Elongation
GA14	0.071	58442	77283	27
GA22	0.028	54351	61756	38

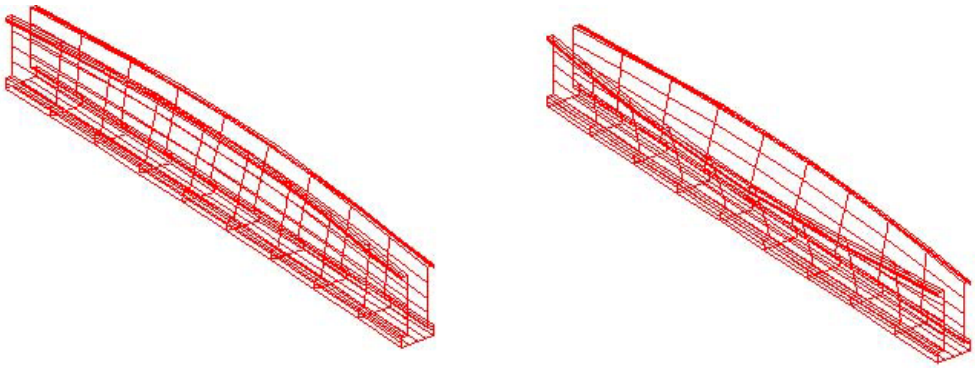

First Mode Second Mode

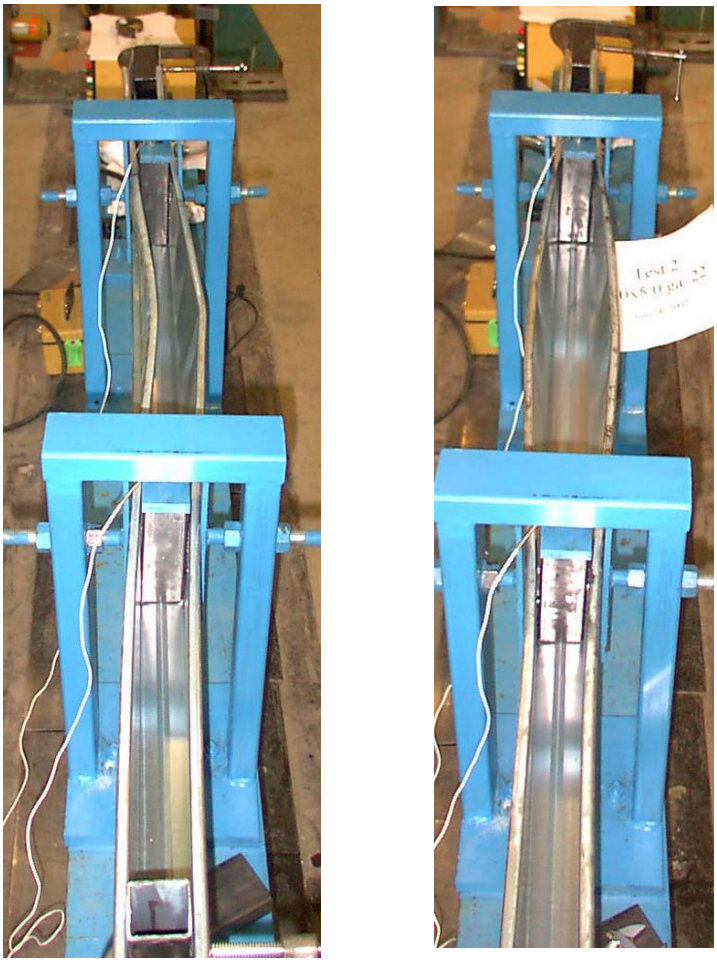

Figure 4.3 First and Second Mode of Distortional Buckling Failure

Table 4.3 Summary of the Test Results

Specimen	GA	Thickness (in.)	Length (in.)	Ultimate Load, P (lbs)				
				Test 1	Test 2	Test 3	Test 4	Average
3.0x5.0	14	0.071	30	1620	1780	1550*	1810	1737
			60	1430	1390	1370	1270	1365
			100	1160	1170	1000	N/A	1110
	22	0.028	30	460	500*	410	475	448
			60	330	310	310	290	310
			100	210	260	230	210	228
2.5x5.0	14	0.071	30	1950	1830	1910	1910	1900
			60	1260	1160	1220	N/A	1213
	22	0.028	30	340	330	350	370	348
			60	320	320	300	N/A	313
3.0x3.5	14	0.071	30	1610	1560	1570	1540	1570
			60	1310	1320	1230	N/A	1287
	22	0.028	30	460	400	370	380	403
			60	310	300	360	280	313
2.5x3.5	14	0.071	30	1580	1680	1690	1440	1598
			60	1220	1150	1170	1120	1165
	22	0.028	30	390	460	420	360	408
			60	280	250	270	N/A	267

* These specimens failed in the second mode of distortional buckling

4.5 DISCUSSION OF RESULTS

The CFS software (2003) was used to calculate the moment capacity, $M_{n,\ AISI}$, according to the NAS (2001). All calculations were based on the yield stress from the tensile coupon tests. The prediction of the inelastic distortional buckling moment capacity, M_{nd}, using both Winter's and Hancock's equations were also calculated. The CUFSM software (Schafer, 2002b) was used to generate the elastic buckling curve to determine the elastic distortional moment, M_{crd}, as input to Eqs. 2.6 through Eqs. 2.9.

In determining M_{crd}, the critical elastic buckling stress for the distortional buckling mode is needed. The geometry of the tested complex hat shape yields

the elastic buckling curve shown in Fig. 4.4-4.5 for GA-14 and GA-22 members respectively. The elastic buckling curve of the first mode does not explicitly show the second minima usually identified as the distortional buckling stress. In deciding the critical elastic distortional buckling stress, consideration of the second mode elastic buckling curve is necessary.

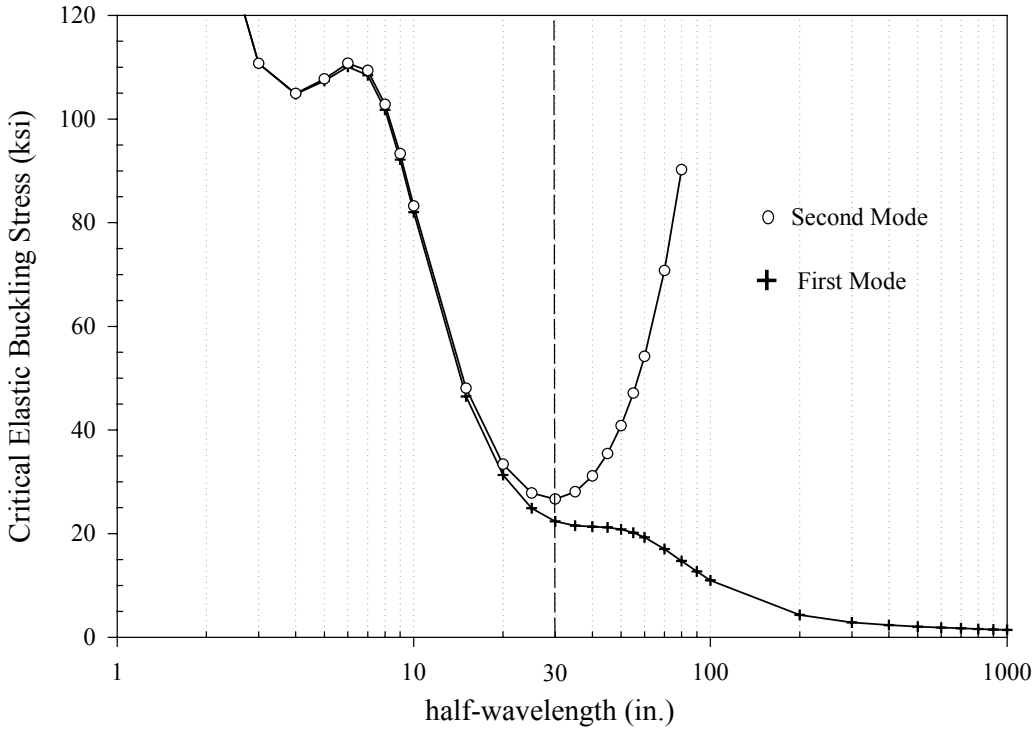

Figure 4.4 Typical Elastic Buckling Curve of Tested Section GA-14 (3.0x5.0)

The elastic buckling curve of the second mode can be plotted to help in deciding the value of the distortional buckling stress. When the elastic buckling stress for a higher mode is close to the first mode stress, such as stresses at unbraced length of 30 in., then the buckling stress of the higher mode must be considered. For the GA-14 section, as shown Fig. 4.4, the minima of the second mode stress occurs at the half-wavelength of 30 in. and has a higher value than the stress at the half-wavelength of 30-in. for the first mode. The lower value of the first mode is taken as the critical elastic buckling stress to calculate the M_{crd}. For the GA-22 section, as shown in Fig. 4.5, the minima of the second mode stress occurs at the half-

wavelength of 50 in. and has a lower value than the critical buckling stress of the first mode at the half-wavelength of 30 in. Therefore, the lower critical distortional buckling stress at the half-wavelength of 50 in. is used to calculate the M_{crd} for the GA-22 specimen with the laterally unbraced length of 30 in. This conservative procedure of choosing the M_{crd} improves the prediction for both Winter's and Hancock's equations.

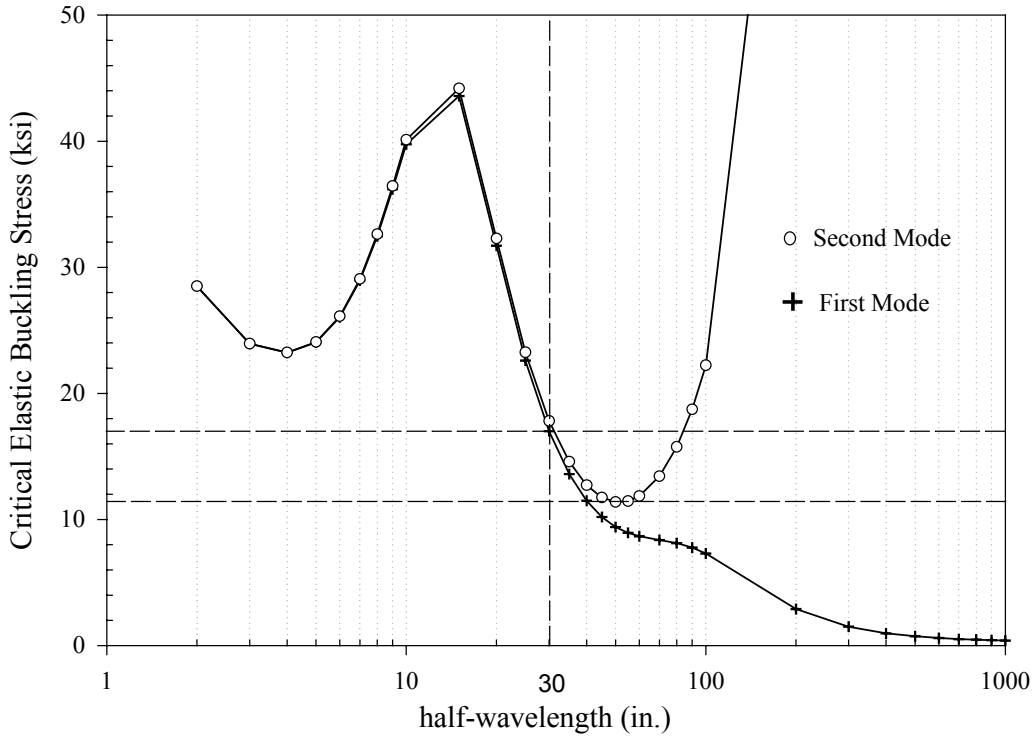

Figure 4.5 Typical Elastic Buckling Curve of Tested Section GA-22 (3.0x5.0)

Three predictions, the NAS (2001), Winter's equation, and Hancock's equations, were compared with the experimental results as shown in Table 4.4a, b, and c. The results in Table 4.4a, b, and c show the ratio between the test moment and predicted moment for 30-in., 60-in., and 100-in. unbraced lengths, respectively. The ratios of the test results to the strength predicted by the NAS (2001) for the GA-22 specimens are found to be as low as 0.438 and 0.555 for the 30-in. and 60-in. unbraced length tests, respectively. This result shows that the NAS (2001) is

unconservative in predicting the flexural behavior at this intermediate length. For the 100-in. beam tests, the NAS (2001) predictions show the best correlation with the test results as shown in Table 4.4c. This agreement is expected because the mode of failure is predominantly lateral or lateral-torsional buckling.

Table 4.4a Performance Predictions for 30 inches Beams

Specimen		Thickness (in.)	Load P, (lb)	M_t (in-kip)	$\frac{M_t}{M_n^{NAS\ (2001)}}$	$\frac{M_t}{M_n^{Winter}}$	$\frac{M_t}{M_n^{Hancock}}$
	14	0.071	1620	32.4	0.633	0.987	1.092
			1780	35.6	0.695	1.084	1.200
			1550	31.0	0.605	0.944	1.045
			1810	36.2	0.707	1.103	1.220
3.0x5.0	22	0.028	460	9.2	0.573	0.923	1.076
			500	10.0	0.623	1.003	1.170
			410	8.2	0.511	0.823	0.959
			475	9.5	0.592	0.953	1.111
2.5x5.0	14	0.071	1950	39.0	1.040	1.535	1.705
			1830	36.6	0.976	1.440	1.600
			1910	38.2	1.018	1.503	1.670
			1910	38.2	1.018	1.503	1.670
2.5x5.0	22	0.028	340	6.8	0.451	0.688	0.799
			330	6.6	0.438	0.668	0.776
			350	7.0	0.464	0.708	0.823
			370	7.4	0.491	0.749	0.870
3.0x3.5	14	0.071	1610	32.2	1.112	1.343	1.417
			1560	31.2	1.077	1.301	1.373
			1570	31.4	1.084	1.309	1.382
			1540	30.8	1.063	1.284	1.355
3.0x3.5	22	0.028	460	9.2	0.797	1.214	1.335
			400	8.0	0.693	1.055	1.161
			370	7.4	0.641	0.976	1.074
			380	7.6	0.659	1.002	1.103
2.5x3.5	14	0.071	1580	31.6	1.228	1.388	1.470
			1680	33.6	1.306	1.476	1.563
			1690	33.8	1.314	1.484	1.572
			1440	28.8	1.120	1.265	1.340
2.5x3.5	22	0.028	390	7.8	0.767	1.038	1.139
			460	9.2	0.905	1.225	1.343
			420	8.4	0.826	1.118	1.226
			360	7.2	0.708	0.959	1.051

Table 4.4b Performance Predictions for 60 inches Beams

Specimen		Thickness (in.)	Load P, (lb)	M_t (in-kip)	$\frac{M_t}{M_n^{NAS\ (2001)}}$	$\frac{M_t}{M_n^{Winter}}$	$\frac{M_t}{M_n^{Hancock}}$
	14	0.071	1430	28.6	0.923	0.928	1.040
			1390	27.8	0.898	0.902	1.011
			1370	27.4	0.885	0.889	0.996
			1270	25.4	0.820	0.824	0.923
3.0x5.0	22	0.028	330	6.6	0.632	0.748	0.895
			310	6.2	0.593	0.703	0.840
			310	6.2	0.593	0.703	0.840
			290	5.8	0.555	0.658	0.786
2.5x5.0	14	0.071	1260	25.2	1.564	1.155	1.323
			1160	23.2	1.440	1.064	1.218
			1220	24.4	1.514	1.119	1.281
2.5x5.0	22	0.028	320	6.4	0.823	0.774	0.933
			320	6.4	0.823	0.774	0.933
			300	6.0	0.772	0.726	0.875
3.0x3.5	14	0.071	1310	26.2	1.360	1.294	1.405
			1320	26.4	1.371	1.304	1.416
			1230	24.6	1.277	1.215	1.319
3.0x3.5	22	0.028	310	6.2	0.850	0.951	1.077
			300	6.0	0.823	0.920	1.042
			360	7.2	0.987	1.104	1.251
			280	5.6	0.768	0.859	0.973
2.5x3.5	14	0.071	1220	24.4	1.841	1.400	1.555
			1150	23.0	1.735	1.319	1.466
			1170	23.4	1.765	1.342	1.491
			1120	22.4	1.690	1.285	1.427
2.5x3.5	22	0.028	280	5.6	1.055	0.944	1.084
			250	5.0	0.942	0.843	0.968
			270	5.4	1.017	0.911	1.046

The statistical analyses of these comparisons can be used to better analyze the test results. The mean, standard deviation, coefficient of variation, and resistance factor (Φ) of the comparison ratios in Table 4.4 are tabulated in Table 4.5a and b. The resistance factors were calculated based on the reliability index (β) of 2.5 according the NAS (2001) procedure, which is shown in Appendix A. Table 4.4a shows the overall performance of each method and Table 4.5b shows the comparison of the results between GA-22 and GA-14 specimens.

Table 4.4c Performance Predictions for 100 inches Beams

Specimen		Thickness (in.)	Load P, (lb)	M_t (in-kip)	$\frac{M_t}{M_n^{NAS\ (2001)}}$	$\frac{M_t}{M_n^{Winter}}$	$\frac{M_t}{M_n^{Hancock}}$
	14	0.0713	1160	23.2	1.864	0.964	1.134
			1170	23.4	1.880	0.972	1.144
			1000	20.0	1.607	0.831	0.978
3.0x5.0	22	0.0283	210	4.2	0.912	0.515	0.626
			260	5.2	1.129	0.637	0.774
			230	4.6	0.998	0.564	0.685
			210	4.2	0.912	0.515	0.626

Table 4.5a Overall Statistical Analysis

30 in. Beam (32 Tests)				
	$M_t/M_n^{NAS\ (2001)}$	M_t/M_n^{Winter}	$M_t/M_n^{Hancock}$	$M_t/M_n^{Proposed}$
Mean	0.817	1.127	1.240	1.145
Std. Dev.	0.263	0.259	0.261	0.203
C.O.V.	32.2%	23.0%	21.0%	17.8%
Phi	0.60	0.72	0.74	0.79
60 in. Beam (28 Tests)				
Mean	1.083	0.988	1.122	1.124
Std. Dev.	0.394	0.227	0.230	0.171
C.O.V.	36.4%	23.0%	20.5%	15.2%
Phi	0.54	0.71	0.75	0.82
100 in. Beam (7 Tests)				
Mean	1.329	0.714	0.852	1.200
Std. Dev.	0.441	0.204	0.230	0.236
C.O.V.	33.2%	28.6%	27.0%	19.6%
Phi	0.49	0.55	0.58	0.70
30 & 60 in. Beam Including LaBoube (2001) (99 Tests)				
Mean	0.854	1.031	1.159	1.129
Std. Dev.	0.420	0.259	0.263	0.216
C.O.V.	49.1%	25.2%	22.7%	19.2%
Phi	0.42	0.70	0.73	0.78

For the 30-in. and 60-in. tests, the NAS (2001) predictions yield the resistance factors of 0.60 and 0.54, respectively. Winter's equation and Hancock's equation yield the resistance factors of 0.72 and 0.75, respectively. The mean values of the three comparisons indicate that Hancock's equation is the most conservative and

the most reliable of the three predictions. The experimental results by Baur and LaBoube (2001) on 24-in. and 48-in. unbraced lengths are included with the 30-in. and 60-in. unbraced length results in this experimental program for the overall statistical analyses shown in Table 4.5a. The Hancock equation is the most conservative and reliable with the mean of 1.16 and the resistance factor of 0.73.

The statistical analyses by thickness, as shown in Table 4.5b, indicate that all three predictions show good agreement, with the mean value higher than 1.0. Because the GA-14 (0.071 in.) specimen has width to thickness ratio 2.5 times higher than the GA-22 (0.028) specimen, the GA-14 specimen will likely be influenced less by the effect of distortional buckling. Hancock's equation still yields the most conservative and reliable of the three predictions, with a resistance factor as high as 0.80.

Table 4.5b Statistical Analysis By Thickness (GA-14 and GA-22)

30 in. Beam (16 Tests Each)								
	$M_t/M_n^{NAS\ (2001)}$		M_t/M_n^{Winter}		$M_t/M_n^{Hancock}$		$M_t/M_n^{Proposed}$	
	14-GA	22-GA	14-GA	22-GA	14-GA	22-GA	14-GA	22-GA
Thickness (in.)	0.071	0.028	0.071	0.028	0.071	0.028	0.071	0.028
Mean	1.000	0.634	1.309	0.944	1.417	1.063	1.246	1.044
Std. Dev.	0.225	0.143	0.19	0.175	0.206	0.177	0.21	0.14
C.O.V.	23%	23%	15%	19%	15%	17%	17%	13%
Phi	0.71	0.71	0.82	0.76	0.82	0.79	0.78	0.83
60 in. Beam (14 Tests Each)								
Mean	1.363	0.802	1.146	0.83	1.276	0.967	1.216	1.031
Std. Dev.	0.356	0.163	0.194	0.125	0.207	0.124	0.187	0.088
C.O.V.	26%	20%	17%	15%	16%	13%	15%	9%
Phi	0.65	0.73	0.78	0.81	0.79	0.83	0.8	0.88
100 in. Beam (3 Tests for 14-GA, 4 Tests for 22-GA)								
Mean	1.784	0.988	0.922	0.558	1.085	0.678	0.950	1.387
Std. Dev.	0.153	0.103	0.079	0.058	0.093	0.070	0.040	0.037
C.O.V.	9%	10%	9%	10%	9%	10%	4%	3%
Phi	0.76	0.77	0.76	0.77	0.76	0.77	0.88	0.91

Based on the test data in this experimental program and those reported by Baur and LaBoube (2001), the statistical analyses can be used to find the better equation to predict the test data by using the same parameters. The parameters used in the equation are the yield moment, M_y, and the moment ratio, $\lambda_d = \sqrt{M_y / M_{crd}}$. In attempting to use the same inverse polynomial equations, none of the coefficients gives a significantly better fit to the available data than the others. Therefore, the proposed equation used to fit the data available for the laterally unbraced flexural member is expressed in decay-log term as

For $\lambda_d \leq 1.0$ $\quad M_{nd} = M_y$ (4.1)

For $\lambda_d > 1.0$ $\quad M_{nd} = 0.0135\, e^{\left(\frac{15.0}{\lambda_d + 2.5}\right)} M_y$ (4.2)

This proposed equation is plotted against the test data as shown in Fig. 4.6. The proposed equation increases the transition point of the moment ratio to 1.0 where the distortional moment is equal to the yield moment. If the elastic distortional moment is more than the yield moment, the yield moment is used for the distortional buckling moment. The statistical analyses, shown in Table 4.5, indicate that the proposed equation is the most reliable. Resistance factors of 0.85 and 0.80 are determined for the GA-22 and GA-14 specimens, respectively.

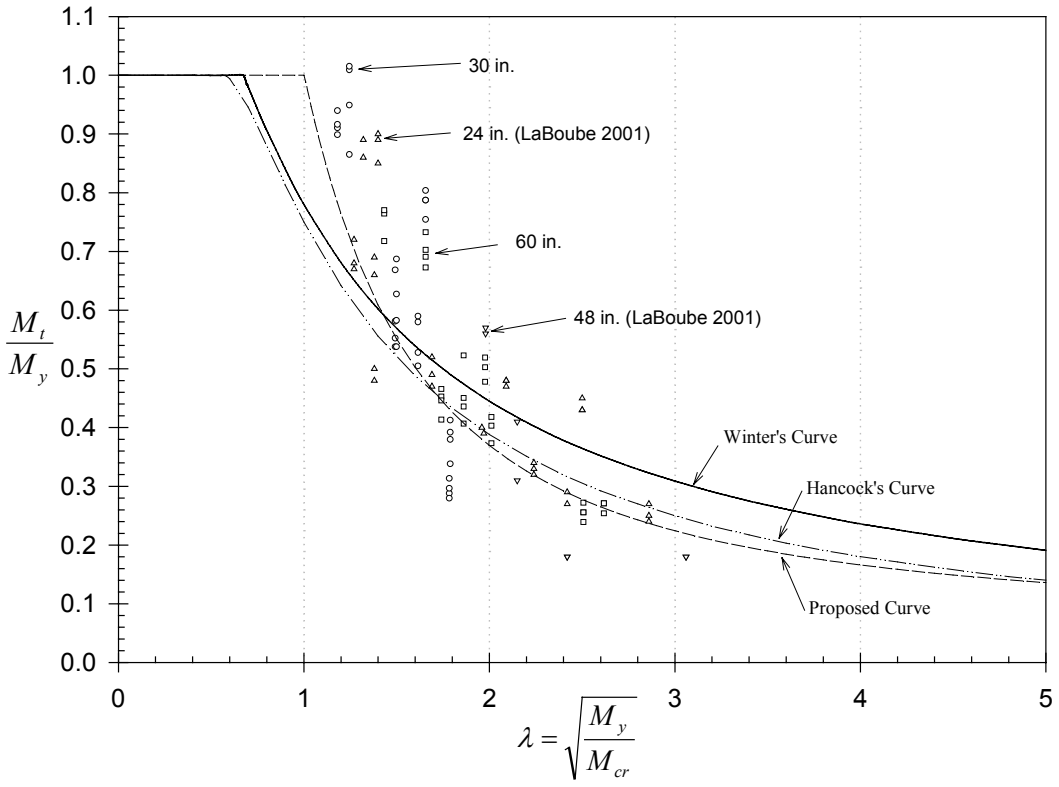

Figure 4.6 Performance of the Test Results

4.6 CONCLUSIONS

Experimental studies on the flexural behavior of a complex hat shape was performed and reported. The analyses using the elastic buckling curve reveal complications regarding the selection of the minima for the critical elastic buckling stress in the distortional buckling mode. The consideration of all modes in deciding the value of the minima for the distortional buckling is important in improving the prediction of Winter's and Hancock's equations. The comparisons of the experimental results with the predictions from the NAS (2001) yield unconservative and less reliable values compared to the predictions by the Winter and Hancock equations, especially for the GA-22 specimens. Hancock's equation is the most conservative and reliable of the three predictions with the overall resistance factor being 0.73. The proposed equation can improve the overall reliability and yields the overall resistance factor of 0.78.

CHAPTER 5

FULL SCALE TESTING OF COLD-FORMED STEEL TRUSSES WITH COMPLEX HAT SHAPE CHORD MEMBER

5.1 INTRODUCTION

Full scale truss testing has been limited to trusses with C-section members, as reported by LaBoube et al. (1998). The previous studies focused on the use of cold-formed steel trusses in the residential construction market. The tested trusses were assembled using C-shaped sections and self-drilling screws. Recently, new technology in rolling cold-formed steel allows the manufacturers to roll a complex hat shape to use as top and bottom chord members. The complex hat shape allows the manufacturers to extend the cold-formed steel roof truss applications into commercial buildings where longer spans are typically used. Full scale testing is necessary for further improvement in safety and efficiency of the newly developed trusses using complex hat shape.

5.2 EXPERIMENTAL STUDY

The objectives of this portion of the study are to experimentally verify the strength and stiffness of a cold-formed steel truss system, as well as, evaluate the behavior and strength of the connections. The results will be compared to calculations made according to the NAS (2001) using the TRUSS D&E (2002) software, which uses a first order stiffness analysis along with the fully effective properties of the cold-formed truss members. The cold-formed steel trusses, as shown in Fig. 5.1, were tested in pairs. The configurations and geometry of the trusses were chosen to represent the typical truss fabricated by the manufacturer. Table 5.1 summarizes the geometric properties of the tested trusses. The test set-up used 19 load application points as shown in the schematic drawing in Fig. 5.2.

Table 5.1 Details of Tested Truss

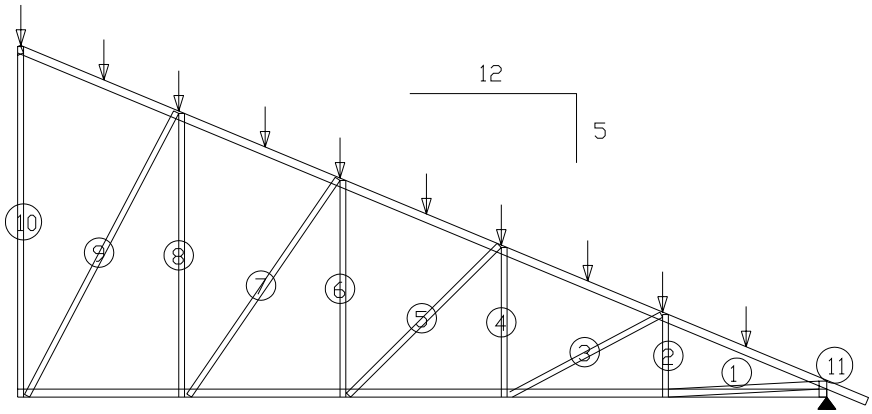

	T1A		T1C		T1	
	Description	Depth (in.)	Description	Depth (in.)	Description	Depth (in.)
Top Chord	SC350-68	3.5	SC500-68	5.0	SC500-68	5.0
Bottom Chord	SC350-54	3.5	SC350-54	3.5	SC350-54	3.5
Web # 1	BW400-54	4.0	NONE	N/A	BW400-54	4.0
Web # 2	C250-27	2.5	C250-27	2.5	C250-27	2.5
Web # 3	C250-27	2.5	C250-45	2.5	C250-27	2.5
Web # 4	C250-27	2.5	C250-27	2.5	C250-27	2.5
Web # 5	BW250-27	2.5	BW250-27	2.5	BW250-27	2.5
Web # 6	C250-27	2.5	C250-34	2.5	C250-27	2.5
Web # 7	BW250-27	2.5	BW250-27	2.5	BW250-27	2.5
Web # 8	C250-54	2.5	C250-54	2.5	C250-54	2.5
Web # 9	BW400-34	4.0	BW400-34	4.0	BW400-34	4.0
Web # 10	BW250-45	2.5	BW250-45	2.5	BW250-45	2.5
Web # 11	BW250-54	2.5	BW600-68	6.0	BW250-54	2.5

Description	Depth (in.)	Thickness (in.)	Area (in^2)	Ix (in^4)	Iy (in^4)
SC350-68	3.5	0.071	0.79	1.16	0.94
SC500-68	5.0	0.071	1.01	2.92	1.17
SC300-54	3.0	0.057	0.64	0.96	0.76
C250-27	5.0	0.028	0.20	0.22	0.11
C250-54	2.5	0.057	0.38	0.42	0.20
BW200-27	2.5	0.028	0.39	0.43	0.23
BW400-34	4.0	0.035	0.57	1.50	0.37
BW250-45	2.5	0.045	0.61	0.67	0.34
BW250-54	2.5	0.057	0.75	0.82	0.42
BW400-54	4.0	0.057	0.92	2.38	0.57
BW600-68	6.0	0.071	1.43	7.54	0.93

Figure 5.1 Test Set-Up

Lateral braces were provided below the top ridge connection. At each load point, a hydraulic ram was used to load through a spreader beam that was supported on top of wood blocks as shown in Fig. 5.3. Load cells were placed and each specimen was loaded to failure, which was defined as the loss of load carrying capacity. The load was controlled manually by applying load through a hydraulic ram and monitored through the load cell.

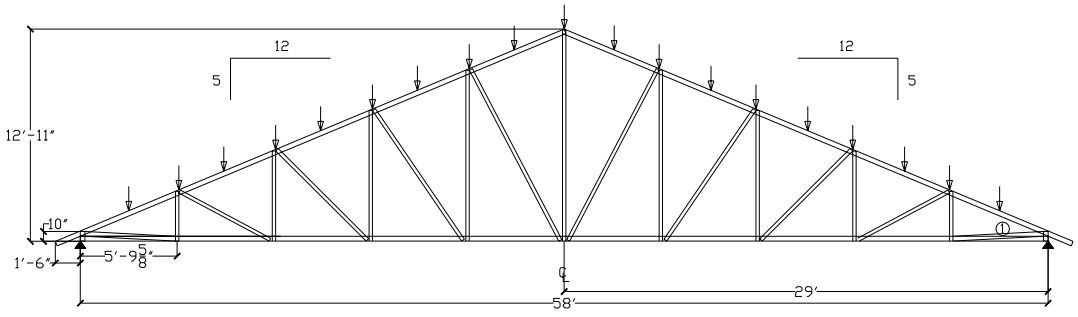

Figure 5.2 Schematic Drawing Test Set-Up

Three different trusses were tested and designated at T1A, T1C and T1 as described in Table 5.1. Two different tests were performed on both T1A and T1C and one test was performed on truss T1. The major objective of testing the T1C truss was to determine the strength and stiffness of the truss when the first diagonal web (web # 1) located next to the support was not included in the design. Both T1 and T1A trusses had the same configuration, except the T1 truss had a 5 in. top chord, instead of a 3.5 in. top chord.

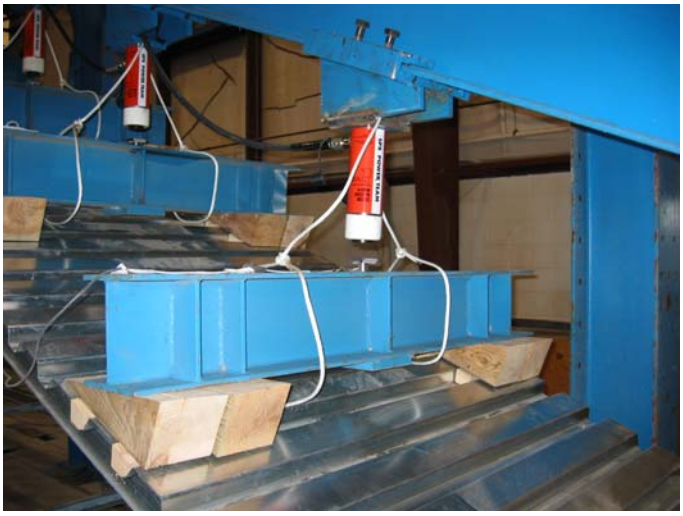

Figure 5.3 Loading Configuration

5.3 RESULTS

5.3.1 T1A RESULTS

T1A-TEST 1

The failure mode of the first test was out-of-plane buckling in diagonal web number 7 as shown in Fig. 5.4. The failure was not expected from the web because the webs are braced out-of-plane when the truss is installed in a building. Thus bracing was omitted in T1A-Test 1. The failed members were replaced on the same truss and cross braces were installed to prevent premature failure of the web. The load was reapplied until failure occurred at the support. The support

rolled out of plane because of the configuration of the load cell as shown in Fig. 5.5. This failure mode was also not expected and a second test of the T1A truss was necessary.

Figure 5.4 T1A Test 1 (First Run) Out-Of-Plane Buckling

Figure 5.5 T1A Test 1 (Second Run) Turning Support

T1A-TEST 2

On the second test, the cross braces were installed on web number 7 and 9 as shown in Fig. 5.6. The braces were installed to prevent the premature failure that occurred in the first test. However, the failure mode of the second test was still out-of-plane buckling of the same web member. The failed members were replaced with new web members on the same truss. The additional cross braces were added to make sure the web would not buckle out-of-plane. The load was reapplied and the failure mode of the second run was the combined bending and compression on the top chord member as shown in Fig. 5.7 and 5.8.

Figure 5.6 T1A Test 2 (First Run) Cross Braces

Figure 5.7 T1A Test 2 (Second Run) Combined Compression and Bending Failure

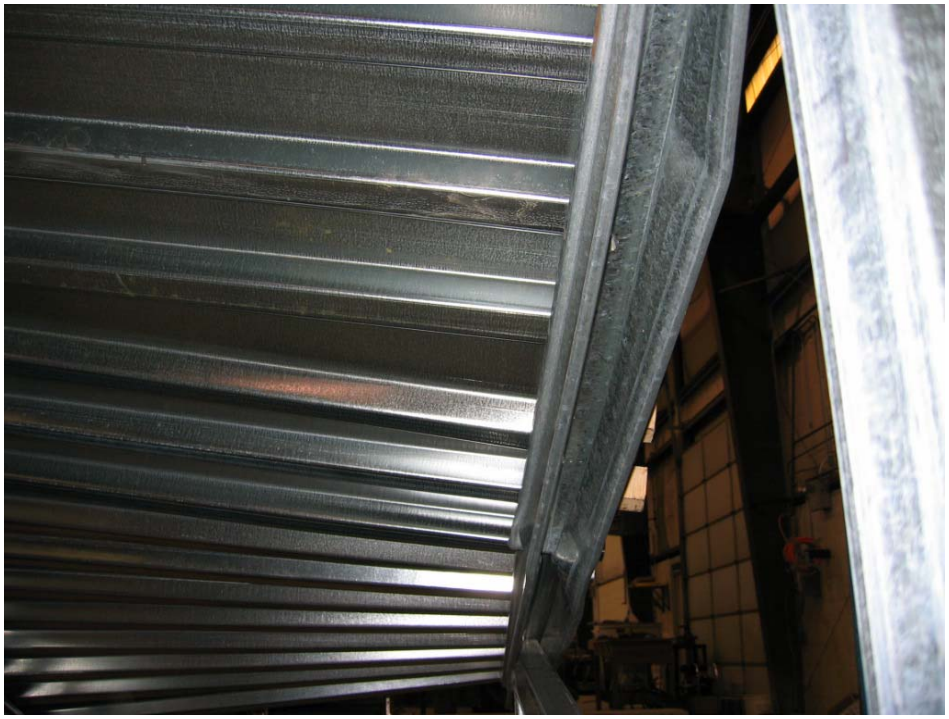

Figure 5.8 T1A Test 2 (Second Run) Combined Compression and Bending Failure

5.3.2 T1C RESULTS

T1C-FIRST TEST

There are two major differences between the T1A truss and T1C truss. The first one is that the T1C truss did not have the first diagonal web member (web #1) next to the support. The purpose of this web is to help transfer load directly to support and reduce the bending moment on top chord member at that location. The second difference is that the T1C truss had 5 in. deep top chords. The test was performed to determine the possibility of leaving this member out to save the labor cost in manufacturing this truss. The failure mode was the failure of top chord member in the distortional buckling mode as shown in Fig. 5.9. The location of the failed top chord member was between web number 11 and web number 2.

Figure 5.9 T1C Test 1 Distortional Buckling Failure

T1C-SECOND TEST

Due to the top chord failure from the first test, T1C, the second test was modified to include a reinforced top chord near the support. The inserted member, which was a double channel box shape, was screwed to the top chord with #10 screws at 12 in. on center. The modification was made to improve the top chord strength and to prevent the failure in a distortional buckling mode. The failure mode of the second test changed from distortional buckling to a local buckling failure of the same top chord member as shown in Fig. 5.10. Once the local buckling failure occurred, the load was applied further and caused the bottom chord member to start a fracture as shown in Fig. 5.11.

Figure 5.10 T1C Test 2 Local Buckling Failure

Figure 5.11 T1C Test 2 Fracture after Local Buckling Failure

5.3.3 T1 RESULTS

The difference between the T1 and T1A trusses was that the T1 trusses had 5 in. top chords. Due to the initial imperfection in the rolling of the box web member, the mode of failure was out-of-plane buckling of web number 7 as shown in Fig. 5.12. The rolled webs did not perfectly nest together and therefore did not act together as a box member.

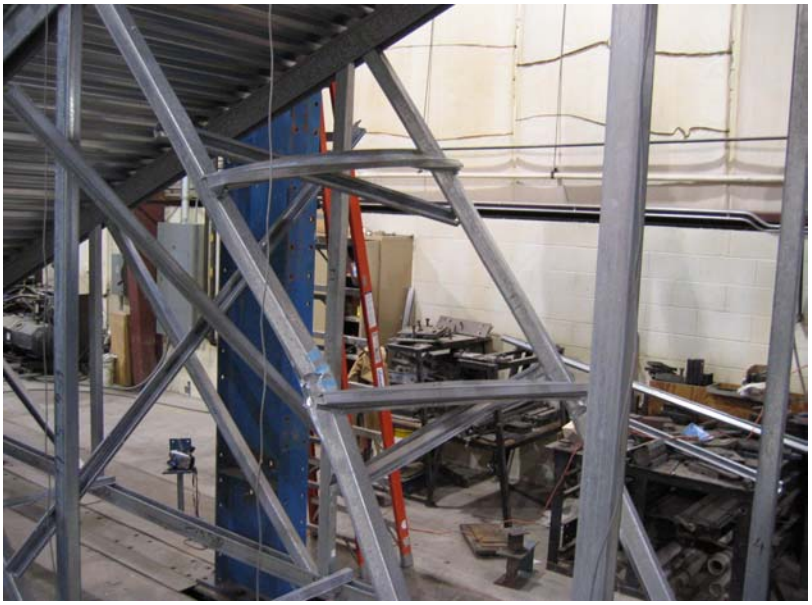

Figure 5.12 T1 Test Out-Of-Plane Buckling due to Initial Imperfection

5.4 DISCUSSION OF RESULTS

GENERAL OBSERVATIONS

From the full scale test, the results reveal important findings that can be used to improve the understanding of the cold-formed steel truss. The first finding that should be mentioned is that the GA-22 web members have shown to be vulnerable to damage during shipping and caused the premature failure especially to out-of-plane buckling. Another observation is that the screw pattern at the top ridge connection as shown in Fig. 5.13 should be required to be placed at the edge of the chord. The edge screws can prevent the end from opening up when sustaining load and caused screws to pull out.

Figure 5.13 Ridge Connection Screws

The 5-in. top chord member distorted elastically more than the 3.5-in. top chord as shown in Fig. 5.14. Because the T1 test failed prematurely at the web, there is no conclusive evidence to show that the truss with a 3.5-in top chord performs better than one with a 5-in. top chord.

Figure 5.14 Distortional Buckling of 5-in Top Chord Member

When using single C-section web members adjacent to each other, the members should be turned so that the screws can be fastened to both sides of the chord member at the same panel point. The unsymmetrical loading can cause the distortion at the panel point as shown in Fig. 5.15. For instance, web numbers 2, 3, and 4, as shown in Table 5.1, are single C-sections. Web number 3 should be turned so that the open end of the section faces the opposite direction of web numbers 2 and 4.

Figure 5.15 Result from One-Sided Screw Pattern at Panel Point

PERFORMANCE OF TRUSSES

The performance of trusses T1A, T1C, and T1 can be summarized in load and deflection plots as shown in Fig. 5.16, 5.17, and 5.18. The T1A and T1 experimental data agrees with the analysis conducted with the commercial software program Truss D&E (2002). The truss models are based on offset nodes at the panel points. The Truss D&E program does not allow the modeling of the T1C truss because of the absence of web # 1. The test result showed that the absence of web # 1 induced significant bending moment at the top chord member near the support and failed the top chord member in distortional buckling mode. All the trusses that were tested exceeded the typical design service load of the roof truss of 40 psf. After the premature failure of the web was prevented, the failure load of the T1A truss was at 2.12 times the service load.

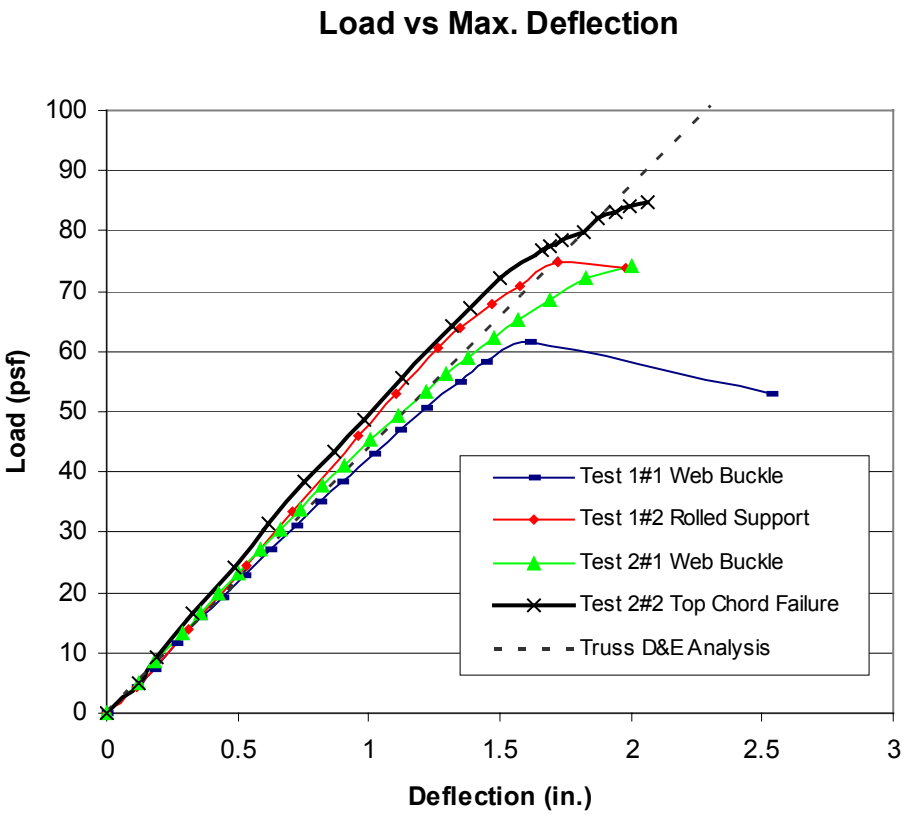

Figure 5.16 Performance of the T1A Trusses

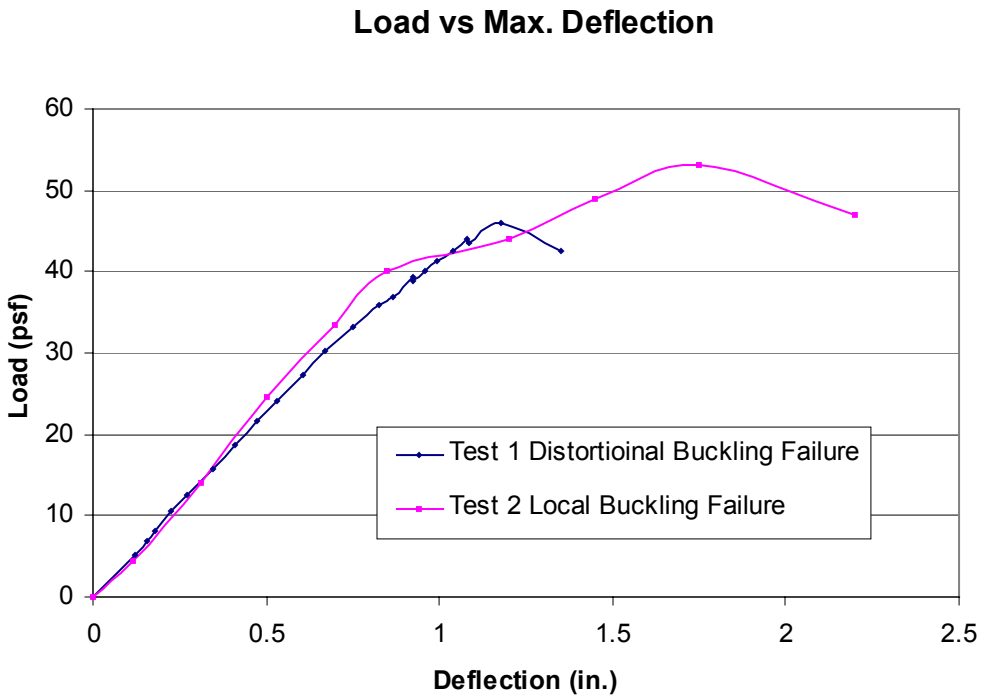

Figure 5.17 Performance of the T1C Trusses

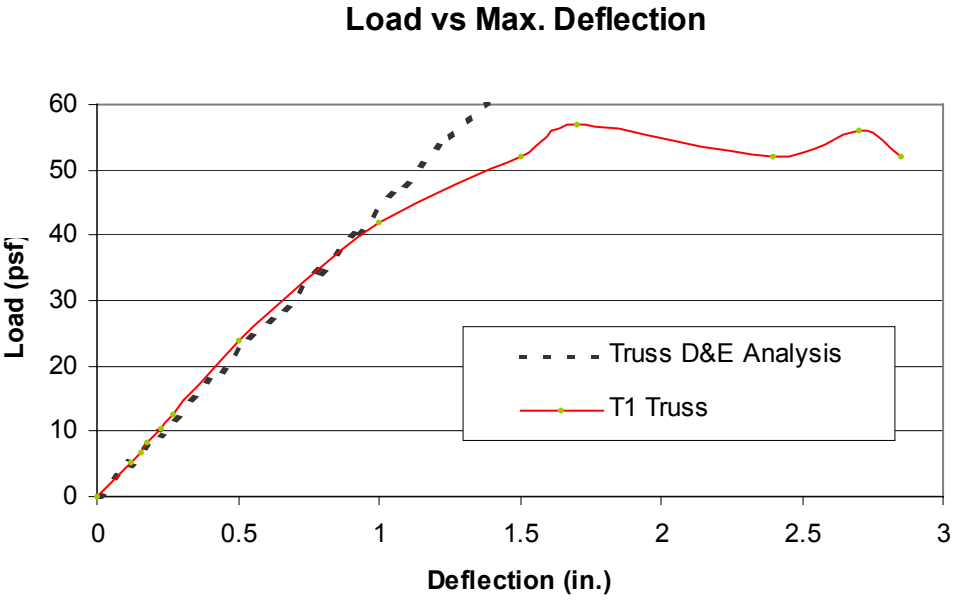

Figure 5.18 Performance of the T1 Truss

5.5 CONCLUSION & RECOMMENDATIONS

The test results showed that the truss performances agreed well with the analyses using Truss D&E when the premature failure of the web is prevented. The attempt to leave out the web number 1 proved to have a significant negative effect on the performance of the truss. The mentioned general observations from the testing can be used to improve the performance of the truss in the future design. The GA-22 web members have shown to be vulnerable to damage during shipping and caused the premature failure especially to out-of-plane buckling. Finally, the performance of 3.5-in. chord member was comparable to that of 5-in. chord members because of the negative effect of the distortional buckling behavior observed in the deeper members.

CHAPTER 6

FINITE ELEMENT STUDY OF COMPLEX HAT SHAPES USED AS TRUSS CHORD MEMBERS

6.1 INTRODUCTION

Finite element modeling can be used to further evaluate the test results and investigate the top chord behavior by considering additional parameters that were not included in the test program. Finite element models of the cold-formed steel complex hat shape members were developed and validated. The finite element model was developed using the commercial finite element software ABAQUS (Hibbitt et al., 1998). The cold-formed steel member was discretized using element S4R from the ABAQUS finite element library. Element S4R is a four-node, general-purpose shell element with finite strain capability (Hibbitt et al., 1998).

6.2 VALIDATION OF FINITE ELEMENT MODEL

A three-dimensional finite element model of the full-scale specimen was created to simulate the test set-up shown in Fig. 4.2. The classical eigenvalue buckling analysis and inelastic postbuckling analysis can be performed for this type of problem. In a classical eigenvalue buckling problem, the analysis will estimate the critical buckling loads as well as useful estimates of collapse mode shapes. The collapse mode shapes can be used to introduce an initial geometric imperfection in the postbuckling analysis (Hibbitt et al., 1998).

In the postbuckling analysis, ABAQUS employs the modified Riks method to perform a load-displacement analysis where other important nonlinear effects,

such as material inelasticity or degree of imperfection, can be included. The modified Riks algorithm is the method suitable for obtaining nonlinear static equilibrium solutions for unstable problems (Hibbitt et al., 1998). The essence of the method is that the solution is viewed as the discovery of a single equilibrium path. The basic algorithm assumes that there is a path-dependent response. For these reasons, it is essential to limit the increment size. In the modified Riks algorithm, the increment size in each iteration is limited by moving a given distance along the tangent line to the current solution point and then searching for equilibrium in the plane that passes through the point. The trigger loads should perturb the structure in the expected buckling modes. Typically, these loads are applied prior to the Riks step. The example of input command and comments on the procedures for ABAQUS analyses is shown in Appendix B.

The end boundary conditions of the model are a pin and roller as shown in Fig 6.1. All nodes in plane A and D are restrained in the directions shown. The lateral brace boundary conditions were applied to the model at both ends (plane A and D) and the end of unbraced length (plane B and C). In the experiment, the lateral braces were provided at each load point by flat plates, but lateral restraint in the FEA applied to nodes in plane B and C, except the nodes in bottom flange. The point loads (P) were also applied symmetrically through nodes in plane B and C. For material nonlinearity, the stress-strain data from coupon tests of the specimens, as shown in Fig 6.2, were converted to the true stress and logarithmic plastic strain and used as an input (Hibbitt et al., 1998).

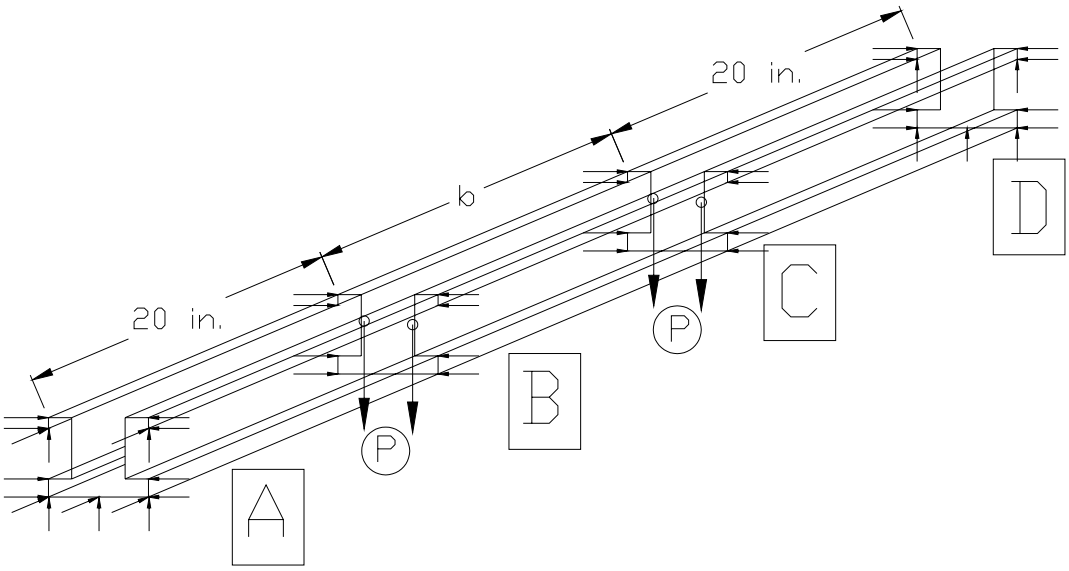

Figure 6.1 Schematic Drawing of FEA Boundary Conditions

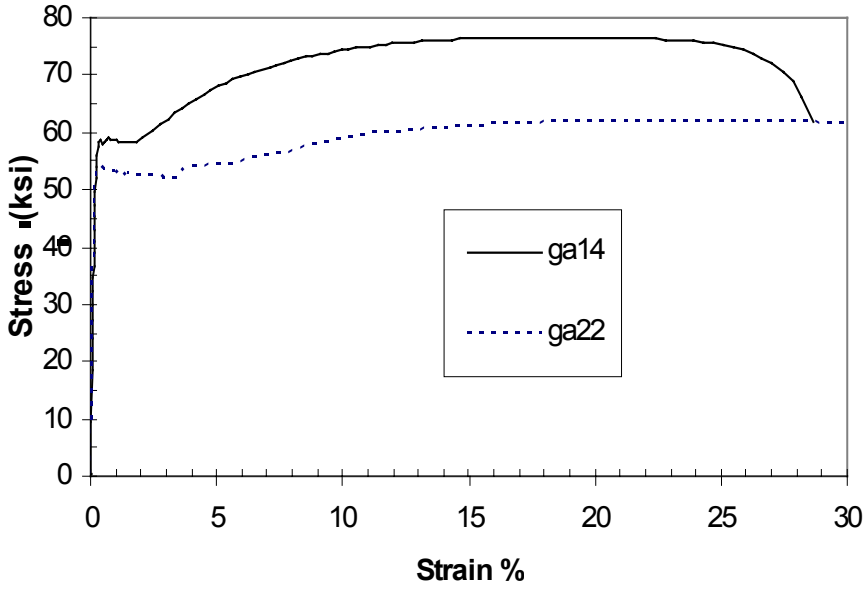

Figure 6.2 Typical Stress-Strain Curve for FEA

The mesh density of finite element models was refined using the ABAQUS built-in options to investigate the adequacy of the number of elements. More refined meshing than the one used in the elastic buckling FEA model did not yield significantly different buckling loads. The visual examination of stress and strain contour plots also showed reasonably smooth plots, therefore, the meshing used throughout the analyses was adequate.

6.3 FINITE ELEMENT STUDY RESULTS

The typical failure mode of the 30-in. and 60-in. unbraced length tests was the first distortional buckling mode shape as shown in Fig. 6.3. From the FEA analyses, the shape of the first mode failure agrees with the tests and is the same for all the analyses. The shapes of the second mode failure are different depending on the thickness and the unbraced length as shown in Table 6.1 and Figure 6.3. Type I of the second mode shape, shown in Fig. 6.3, agreed with each of the 3x5 GA-14 and GA-22 at 30 in. unbraced length tests. The failure in the second mode occurred in some members because of the initial imperfection of the tested specimen.

The results of the elastic FEA are summarized in Table 6.2. The results from the analyses show good comparison with the average from the test results. The elastic buckling loads (P), from both the first and second modes, are calculated because there were second mode failures as mentioned earlier. The elastic FEA results are conservative when compared to the average value of the tests.

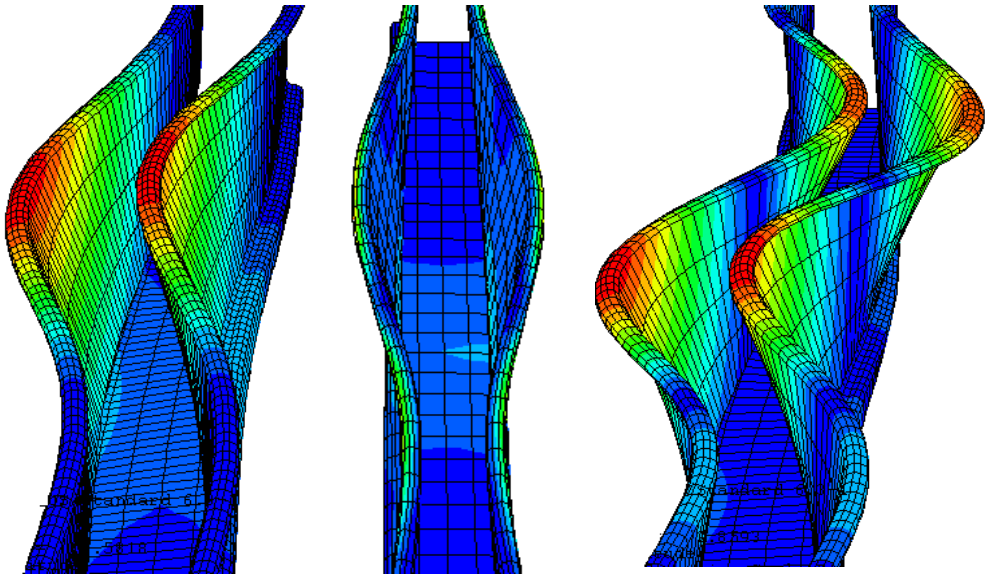

1ST Mode 2ND Mode Type I 2ND Mode Type II

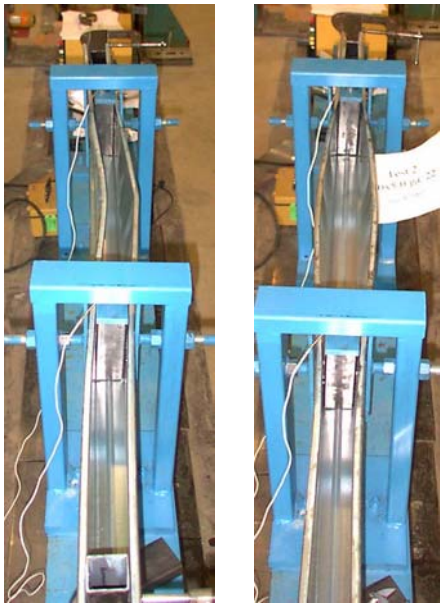

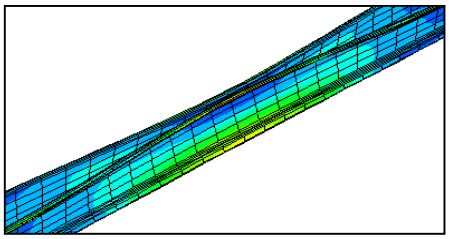

2ND Mode
Type I Inverse

Figure 6.3 FEA and Tests Comparison

Table 6.1 Type of Second Mode Shape

Specimen	GA	Length (in.)	Second Mode Shape (Type)
3.0x5.0	14	30	I
		60	II
	22	30	I
		60	I
2.5x5.0	14	30	I
		60	II
	22	30	I
		60	I
3.0x3.5	14	30	I inverse
		60	II
	22	30	I inverse
		60	II
2.5x3.5	14	30	I inverse
		60	II
	22	30	I inverse
		60	II

Five predictions (the 2001 North American Specification, the Winter equation, the Hancock equation, classical eigenvalue buckling FEA, and inelastic postbuckling FEA) were compared with the experimental results as shown in Table 6.3 and 6.4. The results in Table 6.3 and 6.4 show the ratio between the test moment and predicted moment for 30-in. and 60-in. un-braced length, respectively.

The statistical analyses of these comparisons can be used to better analyze the test results. The mean, standard deviation, coefficient of variation, and resistance factor (Φ) of the comparison ratios are also tabulated in Table 6.3 and 6.4. The resistance factors were calculated based on a reliability index (β) of 2.5 according

the 2001 North American Specification. The determination of Φ is prescribed in the 2001 NAS and is given in App. A. Both elastic FEA and postbuckling FEA analyses yield more reliable values when compared with other methods. The mean values of postbuckling FEA comparison with the tests are 1.10 and 1.26 and the resistance factors (Φ) are the highest at 0.84 and 0.87 for the 30-in. and 60-in. unbraced length tests, respectively.

Table 6.2 FEA Elastic Buckling Results (P)

Specimen	GA	Thickness (in.)	Length (in.)	Test Average (lb)	FEA Elastic Buckling	
					Mode I (lb)	Mode II (lb)
3.0x5.0	14	0.071	30	1737	1693	1923
			60	1365	1286	1424
	22	0.028	30	448	446	461
			60	310	250	310
2.5x5.0	14	0.071	30	1900	1593	1926
			60	1213	1099	1357
	22	0.028	30	348	427	452
			60	313	231	314
3.0x3.5	14	0.071	30	1570	1584	2038
			60	1287	1234	1413
	22	0.028	30	403	359	386
			60	313	233	292
2.5x3.5	14	0.071	30	1598	1438	2094
			60	1165	946	1240
	22	0.028	30	408	337	381
			60	267	204	273

Table 6.3 Performance Predictions for 30 in. Beams

Specimen	GA	Thickness (in.)	$\frac{M_t}{M_n^{FEA}{}_{el}}$	$\frac{M_t}{M_n^{FEA}{}_{inel}}$	$\frac{M_t}{M_n^{Winter}}$	$\frac{M_t}{M_n^{Hancock}}$	$\frac{M_t}{M_n^{AISI}}$
3.0x5.0	14	0.071	0.957	0.997	0.987	1.092	0.633
			1.051	1.095	1.084	1.200	0.695
			0.916	0.954	0.944	1.045	0.605
			1.069	1.114	1.103	1.220	0.707
3.0x5.0	22	0.028	1.031	1.057	0.923	1.076	0.573
			1.121	1.149	1.003	1.170	0.623
			0.919	0.943	0.823	0.959	0.511
			1.065	1.092	0.953	1.111	0.592
2.5x5.0	14	0.071	1.224	1.263	1.535	1.705	1.040
			1.149	1.185	1.440	1.600	0.976
			1.199	1.237	1.503	1.670	1.018
			1.199	1.237	1.503	1.670	1.018
2.5x5.0	22	0.028	0.796	0.819	0.688	0.799	0.451
			0.773	0.795	0.668	0.776	0.438
			0.820	0.843	0.708	0.823	0.464
			0.867	0.892	0.749	0.870	0.491
3.0x3.5	14	0.071	1.016	1.111	1.343	1.417	1.112
			0.985	1.077	1.301	1.373	1.077
			0.991	1.084	1.309	1.382	1.084
			0.972	1.063	1.284	1.355	1.063
3.0x3.5	22	0.028	1.281	1.292	1.214	1.335	0.797
			1.114	1.124	1.055	1.161	0.693
			1.031	1.039	0.976	1.074	0.641
			1.058	1.067	1.002	1.103	0.659
2.5x3.5	14	0.071	1.099	1.176	1.388	1.470	1.228
			1.168	1.251	1.476	1.563	1.306
			1.175	1.258	1.484	1.572	1.314
			1.001	1.072	1.265	1.340	1.120
2.5x3.5	22	0.028	1.157	1.178	1.038	1.139	0.767
			1.365	1.390	1.225	1.343	0.905
			1.246	1.269	1.118	1.226	0.826
			1.068	1.088	0.959	1.051	0.708
Average			1.059	1.100	1.127	1.240	0.817
Std. Dev.			0.141	0.143	0.259	0.261	0.263
C.O.V.			13%	13%	23%	21%	32%
Phi			0.84	0.84	0.71	0.74	0.59

Table 6.4 Performance Predictions for 60 in. Beams

Specimen	GA	Thickness (in.)	$\frac{M_t}{M_n^{FEA}{}_{el}}$	$\frac{M_t}{M_n^{FEA}{}_{inel}}$	$\frac{M_t}{M_n^{Winter}}$	$\frac{M_t}{M_n^{Hancock}}$	$\frac{M_t}{M_n^{AISI}}$
3.0x5.0	14	0.071	1.112	1.181	0.928	1.040	0.923
			1.081	1.148	0.902	1.011	0.898
			1.065	1.131	0.889	0.996	0.885
			0.988	1.049	0.824	0.923	0.820
3.0x5.0	22	0.028	1.320	1.369	0.748	0.895	0.632
			1.240	1.286	0.703	0.840	0.593
			1.240	1.286	0.703	0.840	0.593
			1.160	1.203	0.658	0.786	0.555
2.5x5.0	14	0.071	1.146	1.208	1.155	1.323	1.564
			1.056	1.112	1.064	1.218	1.440
			1.110	1.170	1.119	1.281	1.514
2.5x5.0	22	0.028	1.385	1.441	0.774	0.933	0.823
			1.385	1.441	0.774	0.933	0.823
			1.299	1.351	0.726	0.875	0.772
3.0x3.5	14	0.071	1.062	1.143	1.294	1.405	1.360
			1.070	1.152	1.304	1.416	1.371
			0.997	1.073	1.215	1.319	1.277
3.0x3.5	22	0.028	1.330	1.354	0.951	1.077	0.850
			1.288	1.310	0.920	1.042	0.823
			1.545	1.572	1.104	1.251	0.987
			1.202	1.223	0.859	0.973	0.768
2.5x3.5	14	0.071	1.290	1.348	1.400	1.555	1.841
			1.216	1.271	1.319	1.466	1.735
			1.237	1.293	1.342	1.491	1.765
			1.184	1.238	1.285	1.427	1.690
2.5x3.5	22	0.028	1.373	1.421	0.944	1.084	1.055
			1.225	1.269	0.843	0.968	0.942
			1.324	1.371	0.911	1.046	1.017
Average			1.212	1.265	0.988	1.122	1.083
Std. Dev.			0.134	0.125	0.227	0.23	0.394
C.O.V.			11%	10%	23%	21%	36%
Phi			0.86	0.87	0.71	0.75	0.54

6.4 PARAMETRIC STUDY

The differences in geometric imperfection are used as a parameter to determine the effect on the strength of the specimens. Schafer and Pekoz (1998) recommended the use of a maximum deviation that is approximately equal to the

plate thickness as a simple rule of thumb. In this study, the maximum deviations of the perturbed initial imperfection from the perfect geometry are at 10%, 100% and 150% of the plate thickness. The buckling shapes of Mode I and Mode II are used in the postbuckling analyses to determine the load-displacement curve and the maximum loads are reported in Table 6.5 and 6.6.

Table 6.5 FEA Predictions for First Mode Imperfection

Specimen	GA	Thickness (in.)	Length (in.)	FEA Post Buckling Mode I (lb)		
				10%t	t	150%t
3.0x5.0	14	0.071	30	1625	1393	1343
			60	1211	1105	1081
	22	0.028	30	435	389	377
			60	241	239	238
2.5x5.0	14	0.071	30	1544	1335	1282
			60	1043	973	953
	22	0.028	30	415	375	363
			60	222	222	221
3.0x3.5	14	0.071	30	1449	1242	1201
			60	1146	1050	1017
	22	0.028	30	356	327	314
			60	229	229	227
2.5x3.5	14	0.071	30	1343	1152	1102
			60	905	826	797
	22	0.028	30	331	306	294
			60	197	194	191

From the results, typical plots of the geometric imperfection study are shown in Fig. 6.4 and 6.5. Depending on the initial geometric imperfection, mode II failures can be approximately the same as those of mode I with larger initial geometric imperfections. For example, specimen 3.0x5.0 GA-22, with an initial imperfection of 0.1t in Mode I, has a predicted failure load of 435 lb compared to 405 lb of Mode II as shown in Table 6.5 and 6.6. The comparison helps explain why there were second mode failures in the experiments of the 3x5 specimens.

Table 6.6 FEA Predictions for Second Mode Imperfection

Specimen	GA	Thickness (in.)	Length (in.)	FEA Post Buckling Mode II (lb)		
				10%t	t	150%t
3.0x5.0	14	0.071	30	1886	1688	1654
			60	1415	1205	1178
	22	0.028	30	446	414	405
			60	512	335	353
2.5x5.0	14	0.071	30	1588	1689	1657
			60	1330	1186	1043
	22	0.028	30	444	411	402
			60	363	356	356
3.0x3.5	14	0.071	30	1594	1332	1289
			60	1333	1129	1103
	22	0.028	30	356	327	322
			60	291	230	229
2.5x3.5	14	0.071	30	1452	1333	1287
			60	1191	916	904
	22	0.028	30	340	331	315
			60	273	255	198

The geometric imperfections tend to have little effect on the strength of GA-22 specimens at the unbraced length of 60 in. The same trend also applies to the GA-22 specimens at the unbraced length of 30 in. for 3x3.5 and 2.5x3.5 members. These specimens have smaller width to thickness ratios than the others, where the geometric imperfection yields greater effect toward their strength. In other words, a specimen that tends to fail in a distortional buckling mode also tends to be more sensitive to geometric imperfections. These specimens are those with an unbraced length of 30 in. and high width to thickness ratios.

Another interesting observation from the postbuckling analyses of the second mode shape is the evaluation of the type II failure, which is shown in Fig. 6.3. When imposing the geometric imperfection of the second mode type II on the perfect geometry, some of the analyses, especially the ones with 150%t

imperfection, ultimately failed in the first mode. The final failure of the postbuckling analyses turned out to be a first mode failure even when the initial geometric imperfection was imposed as the second mode type II.

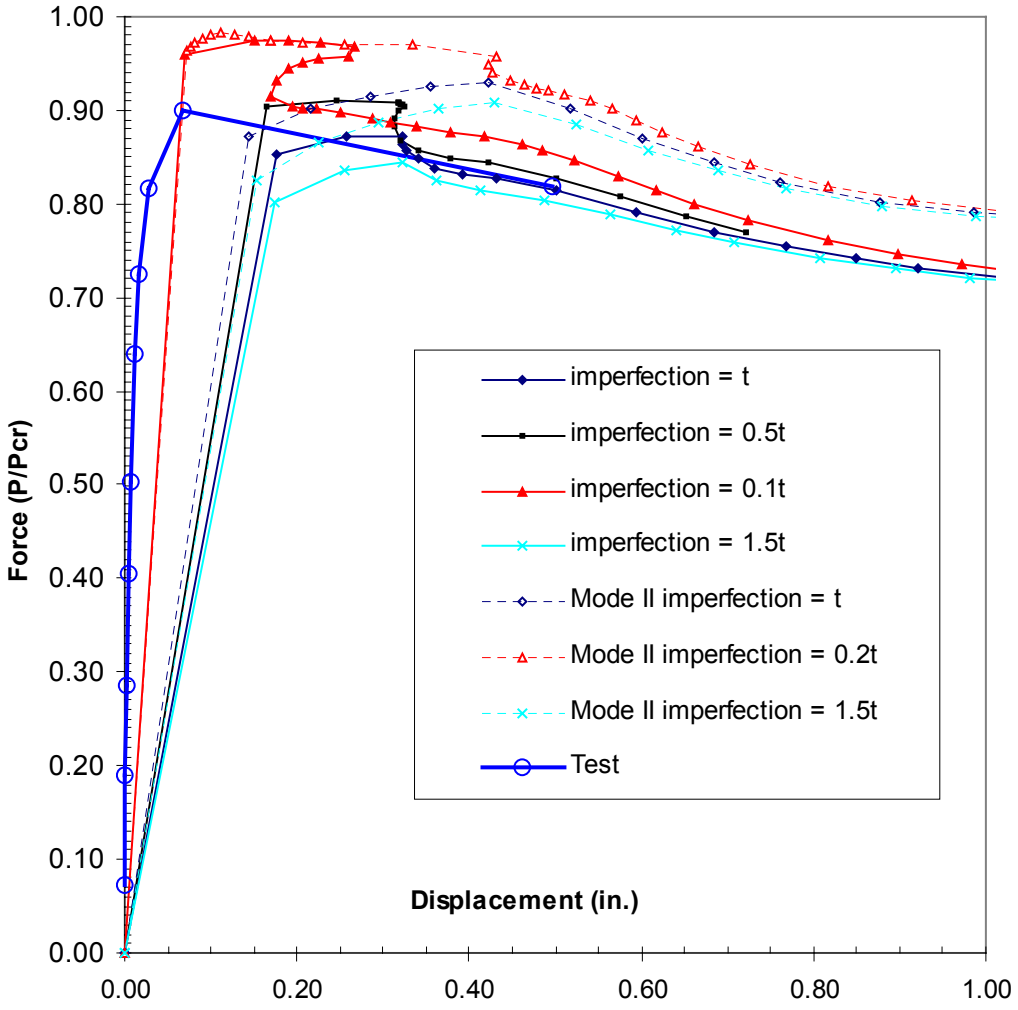

Figure 6.4 Force vs Displacement Plot of Chord
3x5 GA-22 @30 inch

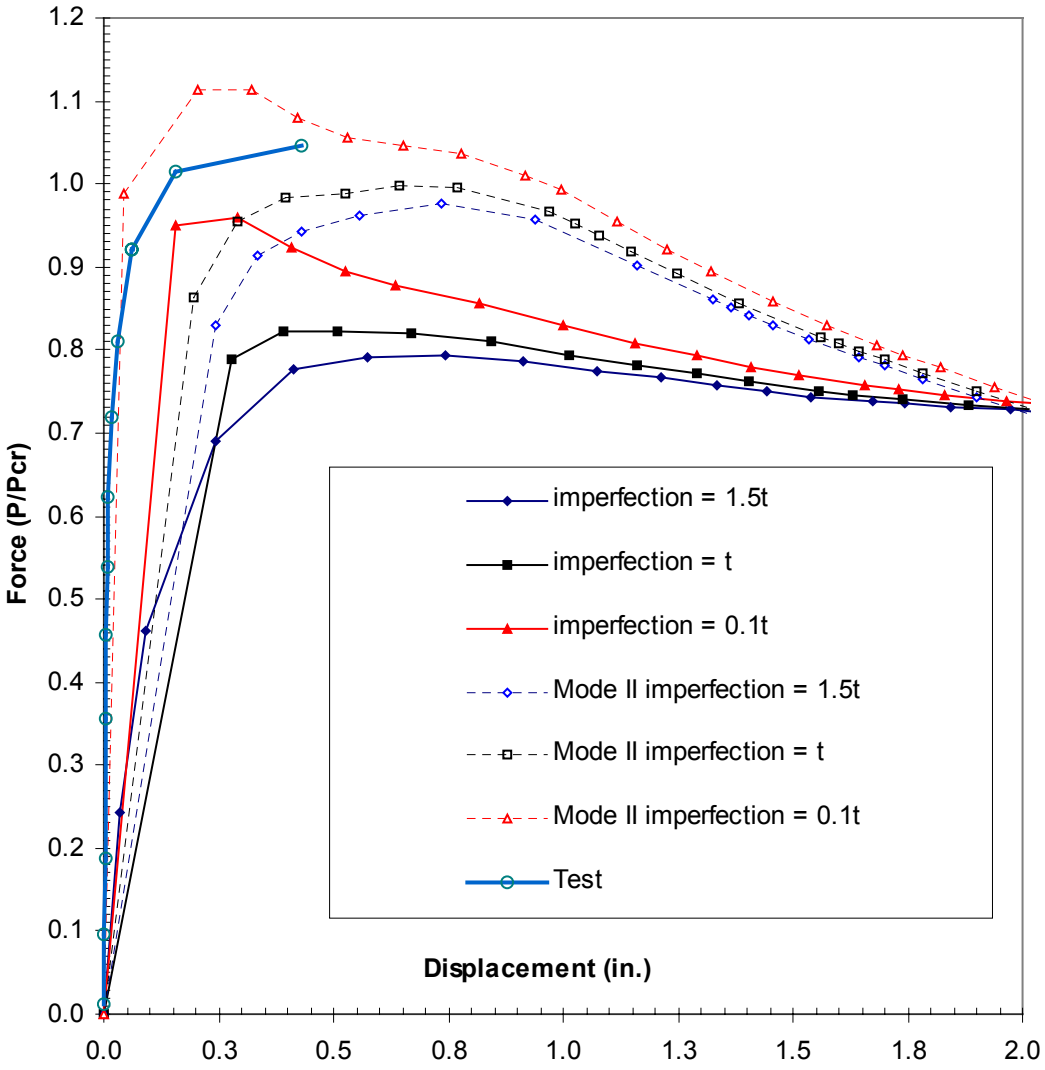

Figure 6.5 Force vs Displacement Plot of Chord
3x5 GA-14 @30 inch

6.5 CONCLUSIONS

The comparisons of the experimental results with the predictions from the 2001 North American Specification yield unconservative values and less reliable compared to the predictions by Winter's equation, Hancock's equation, and FEA especially with the GA-22 specimens. Both elastic FEA and postbuckling FEA analyses yield more reliable results when compared with other methods. The resistance factors (Φ) from the post buckling FEA are the highest at 0.84 and 0.87

for the 30-in. and 60-in. unbraced length tests, respectively. The parametric study on the geometric imperfection also shows that the geometric imperfection has significant effect on the strength and the failure mode shapes in certain specimens.

CHAPTER 7

SUMMARY, CONCLUSIONS AND RECOMMENDATIONS

7.1 SUMMARY

The purpose of this research project was to experimentally and analytically evaluate the behavior of a cold-formed steel roof truss system including the chord, web members as well as the full scale truss. Stub column tests were performed on the web members. The results satisfy the predicted values using the NAS (2001). By using the nested channel sections, the inelastic local buckling failure mode occurred. In longer columns, further experimental and analytical studies are needed for nested C-sections. The complete truss tests were performed and the results compared well with the predicted values calculated according the NAS (2001). Recommendations from the testing observations are made in Chapter 5.

The majority of effort was concentrated on the bending behavior of the laterally unbraced complex hat shaped members used as a truss chord member. The experimental data was based on the results of 67 bending tests performed at Virginia Tech. Additional data from bending tests at the University of Missouri at Rolla were also included in the statistical analyses. Based on the test data in this experimental program and those reported by Baur and LaBoube (2001), statistical analyses were performed to find a better equation to predict the test data, while using the same parameters. The parameters used in the equation are the yield moment, M_y, and the moment ratio, $\lambda_d = \sqrt{M_y / M_{crd}}$. The proposed equation used to fit the data available for the laterally un-braced flexural member is expressed in decay-log form as shown in Eqs. 4.1-4.2. The proposed equation yields the highest resistance factors of 0.85 and 0.80 for 22ga and 14ga

specimens, respectively. The Winter and Hancock equations can also be used to predict the flexural strength more accurately than the NAS (2001).

Finite element analysis of the chord members in bending was performed. The comparisons between the finite element and the test data showed that the finite element method is the most reliable among the comparisons with the 2001 AISI Specifications and Finite Strip Method. Parametric Studies including material nonlinearity and geometric imperfections are investigated. The affect of the geometric imperfections were reported to have significant effect toward the flexural strength of complex hat shape in certain configurations and thicknesses especially the members with larger width-to-thickness ratio.

7.2 CONCLUSIONS

Conclusions on this research on the cold-formed steel roof truss can be listed as follows:

- The analyses using the elastic buckling curve revealed complications regarding the selection of the minima for the critical elastic buckling stress for the distortional buckling mode. The consideration of all modes in deciding the value of the minima for the distortional buckling is important in improving the prediction of Winter's and Hancock's equations.
- Comparisons of the experimental results with the predictions from the 2001 North American Specification indicate that the AISI Specification is unconservative and less reliable compared to the predictions by the Winter and Hancock equations, especially for the GA-22 specimen.
- Hancock's equation is the most conservative and reliable of the three predictions with the overall resistance factor of 0.73.

- A proposed equation can improve the overall reliability and yields the overall resistance factor of 0.78.
- Both elastic FEA and postbuckling FEA analyses yield more reliable values when compared with other methods. The resistance factors (Φ) from the post buckling FEM are the highest at 0.84 and 0.87 for the 30-in. and 60-in. unbraced length tests, respectively.
- The parametric study on the geometric imperfection also shows that the geometric imperfections have significant effect on the strength and the failure mode shapes in certain specimens.

7.3 RECOMMENDATIONS

Based on conclusions from the research, the following recommendations are made:

- The AISI Specifications should provide a separate check for flexural strength against distortional buckling failure for laterally unbraced complex hat shape members.
- The Direct Strength Method (DSM) can be used to improve the current AISI Specifications in determining the flexural strength of laterally unbraced complex hat shape members. Therefore, one should consider all modes in determining the elastic buckling minima for calculating the distortional buckling stress for use in the DSM.
- The parametric study on the geometric imperfection shows that the geometric imperfection has significant effect toward the strength and the failure mode shapes in some specimens. Therefore, the design procedure should include the procedure that accounts for the effect of geometric imperfection.

Suggestions for future research on the cold-formed steel roof trusses can be listed as follows:

- Conduct long column tests of the nested C-section to determine the required screw spacing to keep the member from separating caused by distortion and perform as a single box member.
- Conduct finite element analyses to include the behavior of combined compression and bending of the chord member. Different chord configurations have been introduced to the roof truss industry. The modeling should also include these configurations and investigate the optimal shapes for these types of chord member for the cold-formed steel roof trusses.

REFERENCES

AISI/COFS/TRUSS (2001): Standards for Cold-Formed Steel Framing- Truss Design. American Iron and Steel Institute.

AS/NZS (1996). AS/NZS 4600: 1996 Cold-Formed Steel Structures. Standards Australia and the Australian Institue of Steel Construction.

Baur, S.W. and LaBoube, R.A. (2001), "Behavior of Complex Hat Shape Cold-Formed Steel Members", Proceedings of Structural Stability Research Council, 403-417.

CFS Cold-formed Steel Design Software, (2003), Version 4.14, RGS Software, Inc. 2803 NW Chipman Road Lee's Summit, MO.

Cheung, Y.K. (1976). *Finite Strip Method in Structural Analysis,* Pergamon Press, New York.

Cheung, Y.K. and Tham, L.G.(1997). *Finite Strip Method,* CRC Press, Florida.

Galambos, T. V., (1998). *Guide to Stability Design Criteria for Metal Structures*. 5th Edition, Wiley Inc., New York.

Hancock, G.J. (1978), "Local Distortional and Lateral Buckling of I-beams", ASCE *Journal of Structural Engineering*, 104(11), 1787-1798.

Hancock, G. J., Murray, T.M. and Ellifritt, D.S.(2001). *Cold-Formed Steel Structures to the AISI Specification*. Marcell-Dekker, New York, New York.

Hancock, G. J., Kwon, Y.B. and Bernard, E.S.(1994),"Strength Design Curve for Thin-Walled Sections Undergoing Distortional Buckling" *Journal of Const. Steel Res*., Elsevier, 31, 169-186.

Hibbitt, Karlsson and Sorensen, Inc. (1998), *ABAQUS/ Standard User's Manual*, Versioin 6.3.

Ibrahim M. T. (1998) "Behavior of Cold-Formed C-Section Truss Member" Ph.D. Thesis, Alexandria University, Alexandria, Egypt.

Kwon, Y.B. and Hancock, G.J. (1992), "Strength Tests of Cold-Formed Channel Sections Undergoing Local and Distortional Buckling", ASCE *Journal of Structural Engineering*, 118(7).

LaBoube, R.A. and Yu, W.W. (1998), "Recent Research and Developments in Cold-Formed Steel Framing", *Thin-Walled Structures*, 32,19-39.

North American Specification for the Design of Cold-Formed Steel Structural Members NAS (2001), American Iron and Steel Institute, Washington, D.C.

Pekoz T. and Schafer, B.W. (1998), "Computational Modeling of Cold-Formed Steel: Characterizing Geometric Imperfections and Residual Stresses" *Journal of Const. Steel Res*., Elsevier, 47, 193-210.

Polyzois D. and Charnvarnichborikarn P. (1993), "Web-Flange Interaction in Cold-Formed Steel Z-Section Columns" ASCE *Journal of Structural Engineering*, 119(9), 2607-2628.

Schafer, B.W. and Pekoz T. (1999), "Laterally Braced Cold-Formed Steel Flexural Members with Edge Stiffened Flanges" ASCE *Journal of Structural Engineering*, 125(2), 118-127

Schafer, B.W. (2001). "Thin-Walled Column Design Considering Local, Distortional, and Eluer Buckling", Proc. 2001 Structural Stability Research Council., Ft. Lauderdale, Florida.

Schafer, B.W. (2002a), "Local, Distortional, and Euler Buckling of Thin-Walled Columns", ASCE Journal of Structural Engineering, 128(3), 289-299.

Schafer, B.W. (2002b), "Progress on the Direct Strength Method", Proceeding 16th Int'l Spec. Conf. on Cold-Formed Steel Structures, Orlando, Florida, 647-662.

Shanmugam N.E. and Dhanalakshmi M. (2000). "Stub Column Tests on Cold-Formed Steel Angle Sections" Proc. 15th Int. Specialty Conf. on Cold-Formed Steel Struct., St. Louis, Mo, USA, 239-253.

Specification for the Design of Cold-Formed Steel Structural Members (1996), American Iron and Steel Institute, Washington, D.C.

Truss D&E Cold-Formed Steel Truss Design Software, (2002), Version 14, John F. Butts & Associates, Inc. 2480 Vantage Drive, Colorado Springs, CO.

Winter, G. (1968), "Thin-walled structures-Theoretical solutions and test results" Preliminary Publication of the 8th Congress, IABSE, Zurich, Switzerland, 101-112.

Young, B. and Rasmussen, K.J.R., (1998). "Test of Cold-Formed Channel Columns", Proc. 14th Int. Specialty Conf. on Cold-Formed Steel Struct., St. Louis, Mo, USA, 239-264.

Young, B. and Yan J. (2002), “Channel Columns Undergoing Local, Distortional, and Overall Buckling” ASCE *Journal of Structural Engineering*, 128(6), 728-736.

APPENDIX A : RELIABILITY ANALYSIS EXAMPLE CALCULATIONS

The procedure in determining the resistance factor was performed according to the section F1 of the NAS 2001. The reliability calculations were performed as follows:

ϕ = Resistance factor

$$\phi = C_\phi * (M_M * F_M * P_M) * e^{-\beta_O * \sqrt{V^2{}_M + V^2{}_F + C_P V^2{}_P + V^2{}_Q}} \qquad \text{(B-1)}$$

Where C_ϕ = Calibration Coefficient

C_ϕ = 1.52 for the United States

M_m = Mean value of material factor listed in Table F1 for type of component involved

M_m = 1.10 for bending strength

F_m = Mean value of fabrication factor listed in Table F1 for type of component involved

F_m = 1.00 for bending strength

P_m = Mean value of professional for tested component

P_m = 1.00

β_O = Target reliability index

β_O = 2.5 for structural members for United States

V_M = Coefficient of variation of material factor listed in Table F1 for type of component involved

V_M = 0.10 for bending strength

V_F = Coefficient of variation of fabrication factor listed in Table F1 for type of component involved

V_F = 0.05 for bending strength

V_P = Coefficient of variation of test results, but not less than 6.5%

V_Q = Coefficient of variation of load effect

V_Q = 0.21

m = Degree of freedom

m = n-1

n = number of tests

C_P = Correction factor

$$C_P = \frac{(1+1\frac{1}{n})*m}{m-2} \qquad \text{for } n \geq 4, \text{ and 5.7 for n=3}$$

For Example:

For 60 in. beam test, there are a total of 28 tests with the coefficient of variation of the ratio between the test moment over the predicted value by NAS 2001 of 36.4%. The calculations are as follows:

C_P = 1.119

V_P = 0.364 > 0.065

$$\phi = 1.52*(1.1*1.0*1.0)*e^{-2.5*\sqrt{0.1^2+0.05^2+1.119*0.364^2+0.21^2}}$$

ϕ = 0.54

APPENDIX B : ABAQUS INPUT EXAMPLE

```
** MATERIALS
**
*Material, name=steel                    (Define Material Properties)
*Elastic
29500., 0.3
*Plastic                                 (Define Material Nonlinearlity)
 54.447,       0.
 53.701, 0.031369
 65.785, 0.100346
 75.051, 0.189585
 80.659, 0.283746
** ----------------------------------------------------------------
**
** STEP: Step-1                          (Start Elastic Buckling Analysis)
**
*Step, name=Step-1, perturbation
Buckle                          (Command Buckle used for Elastic Buckling)
*Buckle, eigensolver=lanczos
2, , ,
**
** BOUNDARY CONDITIONS          (Define Boundary Conditions)
**
** Name: Load braced Type: Displacement/Rotation
*Boundary, op=NEW, load case=1
_PickedSet37, 1, 1
*Boundary, op=NEW, load case=2
_PickedSet37, 1, 1
** Name: Right roll Type: Displacement/Rotation
*Boundary, op=NEW, load case=1
_PickedSet38, 1, 1
_PickedSet38, 2, 2
*Boundary, op=NEW, load case=2
_PickedSet38, 1, 1
_PickedSet38, 2, 2
** Name: left roll Type: Displacement/Rotation
*Boundary, op=NEW, load case=1
_PickedSet39, 1, 1
_PickedSet39, 2, 2
*Boundary, op=NEW, load case=2
_PickedSet39, 1, 1
_PickedSet39, 2, 2
** Name: right fix Type: Displacement/Rotation
*Boundary, op=NEW, load case=1
_PickedSet40, 3, 3
```

```
*Boundary, op=NEW, load case=2
_PickedSet40, 3, 3
**
** LOADS                          (Define Load to Node Groups)
**
** Name: Load-L   Type: Concentrated force
*Cload
_PickedSet35, 2, -0.083
** Name: Load-R   Type: Concentrated force
*Cload
_PickedSet36, 2, -0.083
**
** OUTPUT REQUESTS
**
*Restart, write, frequency=1
**
** FIELD OUTPUT: F-Output-1
**
*Output, field
*Node Output
U,
*Element Output                   (Define Output)
S, TSHR, MAXSS, ALPHA, SS
*El Print, freq=999999
*Node Print, freq=999999
*node file, global=yes            (Needed for Postbuckling Analysis)
u,
*End Step
** ----------------------------------------------------------------
**
** STEP: Step-2                   (Start Postbuckling Analysis)
**
*imperfection, file=job.fil       (Introduce Initial Imperfection)
                                  (job.fil is the Result From Step 1)
** BOUNDARY CONDITIONS
**
** Name: Load braced Type: Displacement/Rotation
*Boundary, op=NEW, load case=1
_PickedSet37, 1, 1
*Boundary, op=NEW, load case=2
_PickedSet37, 1, 1
** Name: Right roll Type: Displacement/Rotation
*Boundary, op=NEW, load case=1
_PickedSet38, 1, 1
_PickedSet38, 2, 2
*Boundary, op=NEW, load case=2
```

```
_PickedSet38, 1, 1
_PickedSet38, 2, 2
** Name: left roll Type: Displacement/Rotation
*Boundary, op=NEW, load case=1
_PickedSet39, 1, 1
_PickedSet39, 2, 2
*Boundary, op=NEW, load case=2
_PickedSet39, 1, 1
_PickedSet39, 2, 2
** Name: right fix Type: Displacement/Rotation
*Boundary, op=NEW, load case=1
_PickedSet40, 3, 3
*Boundary, op=NEW, load case=2
_PickedSet40, 3, 3
**
** LOADS
**
** Name: Load-L   Type: Concentrated force
*Cload
_PickedSet35, 2, -0.083
** Name: Load-R   Type: Concentrated force
*Cload
_PickedSet36, 2, -0.083
**
*Step, name=Step-2, nlgeom            (Start Modified Riks Analysis)
*Static, riks
1., 1., 1e-05, 1., 2.,
**
** OUTPUT REQUESTS
**
*Restart, write, frequency=1
**
** FIELD OUTPUT: F-Output-2
**
*Output, field
*Node Output
U, RF, CF
*Element Output
S,
**
** HISTORY OUTPUT: H-Output-1
**
*Output, history, variable=PRESELECT
*End Step
```

VITA

Nuthaporn Nuttayasakul was born in Bangkok, Thailand in 1975. The son of General Chayanth and Major General Kajornporn Nuttayasakul. He grew up in Bangkok Thailand and joined the Royal Thai Army when he was 16 years old and received the scholarships to study in the United States after completed the Armed Forced Academy Preparatory School.

Nuthaporn enrolled at Virginia Military Institute in the fall 1994 and graduated with the bachelor degree in Civil Engineering in May 1998. He then attended Stanford University and received master degree in Civil Engineering in 2000. He started to pursue the doctoral degree at Virginia Polytechnic Institute and State University in the Fall of 2000. He will work in the Royal Thai army and take the position as a faculty at the Chulachomklao Royal Military Academy in Thailand after graduation.